Activation of L-type calcium channel in twitch skeletal muscle fibres of the frog

Fabio Francini, Chiara Bencini and Roberta Squecco

Department of Physiological Sciences, University of Florence, 50134 Florence, Italy

1. The activation of the L-type calcium current (I_{Ca}) was studied in normally polarized (−100 mV) cut skeletal muscle fibres of the frog with the double Vaseline-gap voltage-clamp technique. Both external and internal solutions were Ca^{2+} buffered. Solutions were made in order to minimize all but the Ca^{2+} current.

2. The voltage-dependent components of the time course of activation were determined by two procedures: fast and slow components were evaluated by multiexponential fitting to current traces elicited by long voltage pulses (5 s) after removing inactivation; fast components were also determined by short voltage pulses having different duration (0·5–70 ms).

3. The components of deactivation were evaluated after removing the charge-movement current from the total tail current by the difference between two short (50 and 70 ms) voltage pulses to 10 mV, moving the same intramembrane charge. Two exponential components, fast and slow (time constants, $6 \pm 0{\cdot}3$ and 90 ± 7 ms at −100 mV; $n = 26$), were found.

4. The time onset of I_{Ca} was evaluated either by multiexponential fitting to the I_{Ca} activation or by pulses of different duration to test the beginning of the 'on' and 'off' inequality. This was at about 2 ms, denoting that it was very early.

5. The time constants *vs.* voltage plots indicated the presence of four voltage-dependent components in the activation pathway. Various kinetic models are discussed. Models with independent transitions, like a Hodgkin–Huxley scheme, were excluded. Suitable models were a five-state sequential and a four-state cyclic with a branch scheme. The latter gave the best simulation of the data.

6. The steady-state activation curve saturated at high potentials. It had a half-voltage value of $1 \pm 0{\cdot}02$ mV and the opening probability was only $0{\cdot}82 \pm 0{\cdot}2$ at 20 mV ($n = 32$). This result implies a larger number of functional calcium channels than was previously supposed and is in agreement with the number of dihydropyridine (DHP) receptors calculated for the tubular system.

Excitation–contraction (EC) coupling in skeletal muscle is a complex process starting with the sensing of the T-tubule depolarization and ending with Ca^{2+} release from the terminal cisternae of the sarcoplasmic reticulum (SR). The best candidate as the voltage sensor is the dihydropyridine (DHP) receptor of the T-tubule membrane, whereas the Ca^{2+}-release channel is the ryanodine receptor (foot protein) of the SR membrane. Various mechanisms of coupling between the DHP receptor and the opposing foot have been proposed as mechanical (García, Tanabe & Beam, 1994), electrical, by diffusible messengers (for reviews see: Huang, 1988; Ríos & Pizarro, 1991; Schneider, 1994) or by allosteric interactions (Ríos, Karhanek, Ma & González, 1993).

Voltage pulses, applied to skeletal muscle fibres, evoke non-linear capacitive currents (I_{ICM}), called intramembrane charge movement, and the slow inward calcium current (I_{Ca}). In normally polarized skeletal muscle fibres of the frog intramembrane charge movement is resolved into two components, an early, Q_β, and a delayed Q_γ. I_{ICM} is considered to be the electrophysiological manifestation of the voltage-sensing process leading to contractile activation. I_{Ca} is due to L-type Ca^{2+} channels of the T-tubule membrane that are also DHP sensitive. According to Schwartz, McCleskey & Almers (1985) only a few of the DHP receptors are in fact Ca^{2+} channels and so only some of the sensors for EC coupling are also L-type Ca^{2+} channels. The presence of a protein with a dual function, voltage sensor and calcium channel, may have a further effect: the Ca^{2+} influx due to L-type Ca^{2+} channel activation may modulate the opening of the Ca^{2+}-release channel.

Various models have been proposed for voltage-dependent activation of L-type current including a simple Boltzmann equation (Shirokova, González, Ma, Shirokov & Ríos, 1995; for review see McDonald, Pelzer, Trautwein & Pelzer, 1994)

and a Hodgkin–Huxley equation that involves three independent transitions (Sánchez & Stefani, 1983). However, studies of the L-type Ca^{2+} current in cut-end twitch skeletal muscle fibres of the frog suggested a cyclic scheme for I_{Ca} activation (Feldmeyer, Melzer, Pohl & Zöllner, 1990) or a three-state sequential scheme not following a Hodgkin–Huxley equation (Francini, Pizza & Traina, 1992). These two schemes were based on the potentiation and on the faster activation of I_{Ca} during test pulses following conditioning pulses. Moreover, a model for co-operativity in allosteric proteins was used for activation of calcium channels in the A7r5 smooth muscle-derived cell line (Marks & Jones, 1992).

The present work was planned to re-evaluate the kinetics of I_{Ca} activation using a preparation having only L-type calcium channels. Indeed, I_{Ca} was completely blocked by nifedipine (Fig. 2*B* in Francini *et al.* 1992). We introduced original methods to evaluate the time onset of I_{Ca} and the early time course of activation contaminated by I_{ICM} and to resolve the time course of deactivation with I_{ICM} superimposed. Moreover, pulses of long duration (5 s) were used to evaluate the contaminating slow inactivation. Results were analysed according to different types of models. Models with independent transitions, such as the Hodgkin–Huxley model, could not explain our data. A multistep process with at least five states had to be assumed. Two types of models were found suitable to explain the present results: a five-state sequential model and a four-state cyclic model with a branch. The latter provided the best reproduction of data. Some aspects of this work have already been reported in abstract form (Francini, Bencini & Squecco, 1995).

METHODS

Fibre dissection and Vaseline-gap system

Frogs were cold-adapted in a refrigerator at about 4 °C, and killed by decapitation and pithing the spinal cord. Segments of single muscle fibres were dissected from the semitendinosus muscle of *Rana esculenta*. Those with a diameter between 50 and 120 μm were selected for use. Procedures for mounting and voltage clamping the fibres in a double Vaseline-gap system have been previously described (Francini & Stefani, 1989). Briefly, a stretched muscle was exposed to a Ca^{2+}-free, high-K^+ relaxing solution which caused a transient contraction. After the muscle had relaxed, an ~8 mm length of a single fibre was isolated. The fibre segment was transferred to, and slack mounted in, a double Vaseline-gap chamber, where the two cut ends were cut again to produce a shorter fibre segment, about 0·5–1 mm in length in each lateral, intracellular, pool. The length of the fibre in each Vaseline-gap and that in the middle pool, extracellular, was 0·4 mm. Instead of Vaseline, the gaps were made with the grease Glisseal (Borer Chemie, Zuchwil, Switzerland) that improved the seal. To reduce K^+ contamination, as well as electrode polarization, the four agar bridges providing electrical connections were made with, and stored in, solutions similar to those used in the three-compartment chamber: two in a solution similar to the intracellular one, but without MgATP and glucose, and the two remaining in a solution similar to the extracellular one but with no divalent ions. After a suitable period for equilibration, at least 1 h after applying the external and internal solutions, the experiment started. The temperature was 16 °C throughout.

Solutions

The composition of the relaxing solution was (mM): potassium glutamate, 120; $MgCl_2$, 2; ethylene glycol-bis-(β-aminoethylether)-*N,N,N',N'*-tetraacetate disodium salt (Na_2EGTA), 0·1; and 3-(*N*-morpholino)propanesulphonic acid (Mops), 5 at pH 7·15. Internal and external solutions resembled those used in a previous study (Francini *et al.* 1992) with some changes to minimize further ionic currents except for I_{Ca}. To this aim, solutions were designed to be free of Na^+, K^+ and Cl^-. The following blockers of Na^+, K^+ and Cl^- channels were used: tetrodotoxin (TTX) in the external solution for Na^+ channels; 3,4-diaminopyridine (3,4-DAP) and Rb^+ in the external solution, and tetraethylammonium hydroxide (TEA-OH) in both internal and external solutions for K^+ channels; and 9-anthracenecarboxylic acid (9-AC) and SO_4^{2-} for Cl^- channels in the external solution. Moreover, the high concentration of EGTA (60 mM) in the internal solution minimized any Ca^{2+}-dependent current. Both external and internal solutions were Ca^{2+} buffered; the former with L-malate, to prevent tubular Ca^{2+} depletion (Francini & Stefani, 1989), and the latter with EGTA to block muscle contraction. The composition of the solutions was calculated by a computer program developed by Fabiato (1988) using published stability constants (Martell & Smith, 1977). The calculated free Ca^{2+} concentrations were 2 mM in the external solution and 10^{-10} M in the internal solution. The internal solution contained ATP^{2-} and Mg^{2+} in the form of MgATP and $Mg(OH)_2$ and the following calculated concentrations (mM): free Mg^{2+}, 1; MgATP-complex, 2; and free ATP^{2-}, 0·19. Both solutions were designed to have approximately the same osmolarity (250 mosmol l^{-1}). In all solutions Mops was neutralized to pH 7·15 ± 0·05 with TEA-OH.

The composition of the external solution was (mM): free Ca^{2+}, 2; Ca^{2+}, 15·3; Rb^+, 2·5; TEA^+, 145; L-malate^{2-}, 85; SO_4^{2-}, 1·25; 3,4-DAP, 1; TTX, 0·001; 9-AC, 1; and $Mops^-$, 18. The composition of the internal solution was (mM): $EGTA^{2-}$, 60; glutamate$^-$, 13; ATP^{2-}, 2·94; TEA^+, 139; Mg^{2+}, 5; glucose, 5; and $Mops^-$, 20.

All drugs were obtained from Sigma with the exception of TEA and 9-AC (Aldrich-Chemie).

Stimulation, recording and data analysis

Stimulation protocols, acquisition and recording of data were made with two D/A and A/D converters, TL-1 and Digidata 1200, by using pCLAMP programs, versions 5.5.1 and 6 (Axon Instruments). The signals were filtered through an 8-pole Bessel filter set to a −3 dB corner frequency of 10 kHz. The device described in Francini & Stefani (1989) was improved to have faster electronics by which the potential settles in about 150 μs (time constant of about 35 μs). With this charging speed the template correction became unnecessary except for the very beginning of the transient, i.e. the first 150 μs. Since the rate of potential change is extremely fast during the settling time, the A/D converters frequently saturated during the first 0·4–0·8 ms of large test voltage pulses. To record that portion accurately, data were acquired at two different gains (typically 0·25 and 0·5 nA per A/D unit for voltage steps up to −20 mV and beyond, respectively).

The experiments were planned to resolve fast and slow kinetic components of I_{Ca} activation, and then to determine the most suitable kinetic scheme for activation. This involved many problems: the presence of I_{ICM} in the early part of the 'on' and 'off' records; the slow time course of both activation and inactivation of

I_{Ca}; the exploration over a wide voltage range to determine a quasi-full activation of I_{Ca}; and the necessity of long pulses over a wide voltage range that required fibres stable for hours and a large number of sweeps. Consequently, suitable experimental protocols were used: (1) sets of test voltage pulses, 205 ms long, increased in steps of 10 mV, from −155 to 45 mV, useful for a wide exploration of the membrane linearity and to test the block of any ionic current except for I_{Ca}; (2) sets of test voltage pulses, 5 s long, increased in steps of 10 mV, from −85 to 45 mV, sometimes repeated from −80 to 40 mV to explore with more detail the voltage ranges where different I_{Ca} components arose; (3) shorter duration pulses (from 0·5 to 70 ms) increased in steps of 10 mV, from −60 to 10 mV, were chosen to include only the early part of I_{ICM} and I_{Ca} for an evaluation of the early activation time course of I_{Ca}; (4) 50 and 70 ms pulses to 10 mV were used to determine I_{Ca} deactivation. Tail currents at post-pulse potential ranging between −120 and −50 mV were recorded for 600 ms to include the full relaxation of both I_{ICM} and I_{Ca} and to test the presence of slow components.

With short pulses (0·5–70 ms) the A/D conversion interval was 50–100 μs. With long pulses (205 ms and 5 s), to reduce the number of recorded points, two A/D converter sets were used, one for the 'on' and the other for the 'off' current. Both A/D converters worked with two different A/D conversion intervals: the former 50–100 μs, to record in detail the early part of both 'on' and 'off' phases, and the latter 0·4–5 ms, to record either the time course of the slow I_{Ca} activation and inactivation, or the slow components of the tail current. The result was that we had 'on' and 'off' records with the early fast components recorded in detail, as well as a good view of the following slow phenomena.

Test voltage pulses to the desired potential were applied from a holding potential (V_h) of −100 mV. Sets of seven to sixteen steps were repeated twice and the corresponding current traces were averaged. Control pulses were depolarizing steps of 20 mV applied from a V_h of 0 mV. Control records were obtained from steps of duration and conversion intervals equal to those of the test pulse investigated. Sets of ten control current traces were averaged.

Test protocols were bracketed by the control protocol. To allow a full recovery of I_{Ca} from inactivation (Francini *et al.* 1992) and repriming of charge movement (Chandler, Rakowski & Schneider, 1976; Brum & Ríos, 1987) the protocols were introduced at least 5 min after any V_h change and successive voltage test and control steps were separated by 100 and 60 s intervals, respectively. A test-minus-control current trace was obtained by subtracting an averaged scaled control current trace from an averaged test current trace. Since scaling of control current made the test-minus-control currents noisier, we used a synthesized version of the control current. It was constructed by multiexponential fitting plus a constant (for the leak current) to the 'on' current and without such a constant to the 'off' current. Data, currents and their time integrals were normalized by the size of the linear capacitance measured by control pulses. The condition of the fibre was tracked by monitoring the holding current and by applying, every 20–40 min, a 5 s depolarizing pulse to 10 mV from a V_h of −100 mV to test for run-down of I_{Ca}. The fibre was rejected if there was a change in the leak current and/or I_{Ca} amplitude of more than 5% of its initial size. In the present experiments the viability of the preparation was greatly improved, ranging from 150 to 240 min. The solutions were replaced every 40–60 min.

Data fitting and model simulation were done using non-linear curve fitting based on the Marquardt–Levenberg algorithm of the following programs: pCLAMP version 6, Sigmaplot for Windows version 1.02 and Table Curve version 3.10 (Jandel Scientific, CA, USA). The best fit of each individual model was evaluated by the statistical parameters of these programs, i.e. coefficient of determination (r^2), degree of freedom-adjusted r^2, fit standard error and F statistics. Moreover, the dependence of the parameters and Student's t test were used as indicators of the degree of certainty with which the single parameters of the function were determined. To determine which kinetic model best suited the results different models were fitted to the same experimental data. However, visual inspection was not always an adequate substitutive means of comparison especially if two different models (i.e. different order or different number of terms of a polynomial equation) produced fits which were visually very similar. A model was chosen if it showed a significant improvement of F statistics. We also took into account the improved significance of each individual parameter of the compared models and, in particular, the worst parameter of the chosen model had to be better than the worst of the other. A difference showing $P \leqslant 0{\cdot}05$ was considered significant. Data are presented as means ± S.E.M.

RESULTS

Capacitive and ionic currents in test and control voltage steps

Since our goal was to evaluate slow as well as fast kinetics of I_{Ca} activation, all other ionic currents had to be minimized. Moreover, the control pulses needed a potential range that offered not only consistent and linear capacitive properties but also a linear leak and lack of ionic currents. Figure 1 shows current records of a representative experiment in response to test voltage pulses (205 ms long) from a V_h of −100 mV, in steps of 10 mV from −155 to 45 mV (*A*) and currents with rapid decay, as expected for predominantly linear capacitance, in response to 10 and 20 mV control pulses from a V_h of 0 mV (*B*). To assess the lack of ionic currents, except for I_{Ca}, in test traces, as well as leak linearity in control records, values of currents measured at the 'on' end are plotted *vs.* voltage in *C*. The last 10 ms of 'on' current traces were averaged to reduce the error introduced by noise. The plot shows that values of test currents (●) are linearly related to voltage step size in the range from −155 to −65 mV and that the extrapolated linear fit towards more positive potentials matched the data of currents elicited by control pulses (■). These results demonstrate that the solutions used (see Methods) minimized all ionic currents except for I_{Ca} in test traces as well as any ionic current in control traces. Assessment of linear capacitive properties in voltage pulses from 0 mV was made by determining the time integral of the related currents. For each individual fibre these were linearly related to voltage step size, in agreement with previous results (Brum, Fitts, Pizarro & Ríos, 1988; Huang, 1993), denoting the lack of non-linear capacitive current (I_{ICM}). Consequently, the control pulses consistently used were 20 mV depolarizing pulses from a V_h of 0 mV. Data from Fig. 1*C* after the subtraction of the linear fit are reported in *D*. This plot is the I–V curve of I_{Ca} determined at 205 ms. The first value below zero level indicates the voltage threshold for I_{Ca} at −55 mV. This value was confirmed by long pulse (5 s) experiments where a 4-fold larger I_{Ca} was

recorded (see below and Fig. 7*A* for comparison). The mean value for I_{Ca} voltage threshold was -57 ± 2 mV ($n = 45$).

Activation kinetics of I_{Ca}

To determine the activation kinetics of I_{Ca} we used long (5 s) voltage pulses. I_{Ca} showed similar characteristics (time course and voltage dependence) to those observed in previous works (Francini & Stefani, 1989; Francini *et al.* 1992) apart from a shift of the *I–V* curve to 10 mV more negative potential due to the lower free Ca^{2+} concentration used here (2 mM) than before (10 mM). Accordingly, the maximum of the *I–V* curve of I_{Ca} had a lower mean value with respect to many other works (Sánchez & Stefani, 1983; Feldmeyer *et al.* 1990; Feldmeyer, Zöllner, Pohl & Melzer, 1995) where 10 mM Ca^{2+}, a less physiological $[Ca^{2+}]$, was used for a better evaluation of I_{Ca}. The value was 16 ± 3 nA corresponding to $15{\cdot}9 \pm 3$ μA cm^{-2} or $2{\cdot}4 \pm 0{\cdot}3$ μA μF^{-1} if normalized to the apparent surface area of the fibre or to the linear capacitance, respectively ($n = 32$).

The results from a typical experiment are shown in Fig. 2*A*. I_{Ca} is detectable from the −50 mV trace as a downward-going current. For voltage pulses from −50 to −20 mV I_{Ca} increases to a steady value whereas for more depolarizing pulses it has a transient form. A clear delay of I_{Ca} activation is visible in −30 and −20 mV traces. The delay becomes less pronounced as the membrane potential is stepped to progressively more positive potentials. This sigmoidal time course involves the presence of more than a single transition in the activation pathway.

Various sets of calculations were performed to evaluate the kinetics of the time course of I_{Ca} activation and to match the most suitable model to the experimental findings. Two considerations must be made. (1) Owing to the presence of I_{ICM} in the first time segment from the 'on' edge, the kinetics of I_{Ca} could be evaluated only beyond a time at which I_{ICM} was completely relaxed. Taking into account that relaxation time is shorter as voltage increases (see Fig. 3 in Hui, 1991*a*) we assumed that the I_{ICM} time course was complete in 150–200 ms for −50 and −40 mV traces and in 50–100 ms for traces elicited by −30 mV and more depolarizing pulses. Consequently, the multiexponential fit on the time course of I_{Ca} traces was made excluding this time interval. (2) Although inactivation of I_{Ca} was very slow, it significantly affected the time course of activation because this was a slow phenomenon too (e.g. in Fig. 2*A* at −10 mV the time constant of I_{Ca} decay was about 2·5 s and time to peak was about 2 s). Consequently, both processes must be considered.

The first procedure used was a fit to the current traces of models including both activation and inactivation processes. Two models were considered: the Hodgkin–Huxley model,

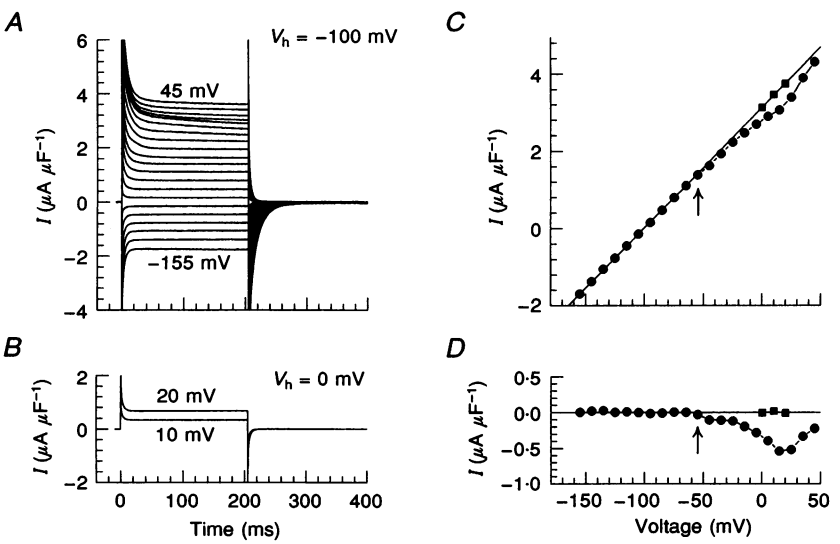

Figure 1. Lack of any ionic current in control traces and lack of any ionic current except for I_{Ca} in test traces

Time course of current traces ('on' and 'off') for test voltage pulses, 205 ms long, from −155 to 45 mV in steps of 10 mV from a V_h of −100 mV (*A*), and for control pulses to 10 and 20 mV from a V_h of 0 mV (*B*). *C*, relation between the current values, determined by the average of the last 10 ms of the 'on', and voltage: ●, data from *A*; ■, data from *B*. The continuous line is a linear fit to data in the range between −155 and −65 mV, which also adequately fits the data at a V_h of 0 mV, denoting lack of any ionic current at these voltages. *D*, same data as in *C* are reported after subtracting the linear fit of *C*; horizontal line is zero level. Voltage threshold for I_{Ca} is at −55 mV, indicated by an arrow in *C* and *D*. In all panels current values are normalized to apparent linear capacitance and units are given as μA μF^{-1}. Fibre A4125, fibre diameter 115 μm, linear capacitance 10·3 nF or 7·15 μF cm^{-2} of apparent lateral fibre surface area.

with independent transitions and fixed rate constants; and a general model, with no fixed rate constants (for involved formalisms see Appendix).

The Hodgkin–Huxley model was tested by eqn (A24). The best fit to current traces of Fig. 2*A* was obtained with $n = 3$ (m^3) and $b = 1$. The m^3 kinetics are in agreement with previous results (Sánchez & Stefani, 1983). In contrast to the prediction of the Hodgkin–Huxley model, inactivation was never complete even at positive potentials.

The general model was tested by multiexponential fitting to transient-type current traces. It gave results with statistical significance when three exponential terms were used (but for some exceptions see below). The time constant of the slowest process had a value comparable to that found for inactivation by means of the Hodgkin–Huxley model (τ_h). For example, for the trace at −10 mV of Fig. 2*A* the values of the slowest time constant and τ_h were 2·5 and 2·45 s, respectively. Even so, the multiexponential fit gave better statistical significance than the Hodgkin–Huxley model for all voltage ranges tested. F statistics for the fitted curves gave $F > 0{\cdot}9995$ and $0{\cdot}99 < F < 0{\cdot}999$, respectively; P values from Student's t test related to each individual parameter were $P < 0{\cdot}001$ and $0{\cdot}5 < P < 0{\cdot}01$, respectively.

In the second procedure activation was fitted after removing the inactivation process in order to improve the fitting procedure. The time course of inactivation was estimated by fitting the function $A'h(V,t)$, whose factors are from eqns (A12*a*) and (A22*b*), to I_{Ca} decay. In agreement with the result of the first procedure and Francini *et al.* (1992), the best fit was obtained with a single exponential function plus a constant. The time constant value was similar (e.g. at −10 mV it was 2·42 s) to the slow time constant found above, confirming that it expressed the time course of inactivation. The results of the fit are superimposed on −10, 0 and 10 mV traces in Fig. 2*A*. The parameter h expresses the fraction of residual open channels not closed by the inactivation process. From eqns (A21*a*)

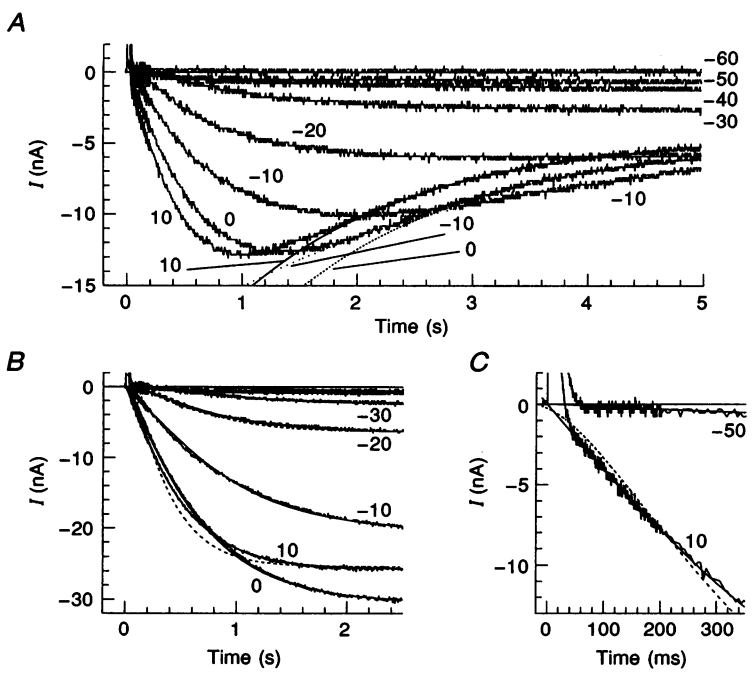

Figure 2. Time course and evaluation of activation kinetics of I_{Ca}

A, current traces (test − control) recorded during 5 s voltage steps, in 10 mV increments, from a V_h of −100 mV: only representative traces from −60 to 10 mV are presented; potentials are indicated by the numbers close to each record. At −50 mV the inward I_{Ca} is observed; from −50 to −20 mV pulses, the current increases progressively up to a steady level. For the −10 to 10 mV traces, the currents are transients showing a decaying phase. A single exponential curve plus a constant fitted to current decay (inactivation phase) are superimposed on traces from −10 to 10 mV (indicated by thin lines). The respective time constants are 2·42 s (−10 mV), 1·64 s (0 mV) and 1·56 s (10 mV). *B*, time course of I_{Ca} activation evaluated by the general model after removal of inactivation from the original traces of *A*; superimposed is the fit (continuous lines) of two (for −40, −30 and −10 mV traces) or three (for −50, −20, 0 and 10 mV traces) exponential functions. Note the different ordinate scale. The −50 and −40 mV traces are not indicated. *C*, detail of −50 and 10 mV traces of *B* to show the appropriate fit for the onset of I_{Ca} activation of the general model. *B* and *C*, dashed lines on −20 and 10 mV traces are the fit of the m^3 Hodgkin–Huxley equation. The horizontal lines are the zero current level. Fibre A3505, diameter 55 μm, linear capacitance 4·55 nF or 6·58 μF cm^{-2} of apparent lateral fibre surface area.

and (A22*a*) the time and voltage dependence of the inactivation gate closing were calculated by the equation:

$$I(V,t) = A'[1 - h(V,t)]. \quad (1)$$

With regard to current traces elicited by low depolarizations (traces from −50 to −20 mV of Fig. 2*A*) we simulated inactivation gate closing using the cyclic model and the parameters of the inactivation pathway reported in Francini *et al.* (1992). According to this work, the sustained and apparently non-inactivating time course of current traces is also contaminated by inactivation even if not detectable by eye.

Inactivation was removed by subtracting the $I(V,t)$ curves from the corresponding current traces of Fig. 2*A* (see eqn (A20)). The results of these differences, representing the time course of activation, are reported in Fig. 2*B*. On these traces we performed a multiexponential fit, eqn (A10), to evaluate I_{Ca} activation kinetics. Equation (A10) as a sum of two exponential functions ($i = 2$) could be fitted with statistical significance to traces elicited at any voltage. When eqn (A10) was as a sum of three exponential functions ($i = 3$) only at some voltages (−50, −20, 0 and 10 mV) were all fitted parameters statistically improved. F statistics for the fitted curves gave $F > 0{\cdot}9995$ and $0{\cdot}99 < F < 0{\cdot}999$, respectively. P values from Student's t test related to each individual parameter were $P < 0{\cdot}001$ and $0{\cdot}5 < P < 0{\cdot}01$, respectively. In contrast, for other voltages the three exponential fit was not resolved because some or all fitted parameters were not statistically significant. This indicated the presence of at least three components. One of these could not be resolved for all voltages because its time constant value was similar to another component. This fact is clearly shown in Fig. 6*B* and *C*, where time constant *vs.* voltage relations are reported. Continuous lines superimposed on traces of Fig. 2*B* are the best fits obtained with two or three exponential functions according to the voltage. Details of −50 and 10 mV traces with superimposed fitted curves are presented in Fig. 2*C* to show the successful fit for the onset of activation. In the first 80–100 ms and about 50 ms after the 'on' edge at −50 and 10 mV, respectively, the divergence between the fitted curve and the corresponding current trace is due to the presence of I_{ICM}. Using the Hodgkin–Huxley equation for activation (eqn (A16)), the best fit was obtained with m^3 but statistical analysis gave the best significance for the fit obtained with eqn (A10) for all voltage ranges tested. Consequently, the Hodgkin–Huxley model was less suitable for describing not only the inactivation but also the activation process. For comparison −20 and 10 mV fits are reported in Fig. 2*B* and *C* as dashed lines.

It is noteworthy that the fit gave a time delay, t_ρ, of 1·5–2·5 ms in the voltage range tested confirming the assumption of a time conduction of depolarization in the tubular system (Simon & Beam, 1985; Huang & Peachey, 1992).

Analysis of the early activation time course of I_{Ca}

The above procedure allowed us to have an indication of the activation kinetics of I_{Ca}, but left uncertainties owing to the presence of I_{ICM} in the first 50–200 ms of the 'on' traces. To verify whether the extrapolated fitted curve predicted the real time course of I_{Ca} activation, I_{ICM} had to be removed from the current traces. A suitable fitting procedure to determine the time course of I_{ICM} could not be used because this was contaminated by the early time onset ($t_0 \approx 2$ ms) of I_{Ca}. Moreover, we used neither Ca^{2+} channel blockers nor low-Ca^{2+} solutions to evaluate I_{ICM} since any intervention aimed to minimize I_{Ca} affected I_{ICM} (Hui, 1991*b*; Ríos & Pizarro, 1991). Therefore, we introduced an original method explained in the Appendix by eqns (A27) to (A31) that allowed us to evaluate I_{Ca}, regardless of the presence of I_{ICM}. This method made use of protocols with pulse durations from 0·5 to 70 ms, in steps of 0·5, 1 and 5 ms increments for pulse duration ranges of 0·5–4, 4–10 and 5–70 ms, respectively. For each pulse duration the sum of the time integrals of the 'on' and 'off' total currents was calculated. This method assumed that the sum of the time integrals of 'on' and 'off' total currents eliminated the charge moved by I_{ICM} under conditions of time integral equality of I_{ICM} at the 'on' and 'off', $Q_{ICM,on}$ and $Q_{ICM,off}$, respectively (cf. eqn (A27)). This condition was tested and confirmed for voltage pulses negative to I_{Ca} threshold (−55 mV) and pulse durations up to 70 ms. As an example, the $Q_{ICM,on}$ and $Q_{ICM,off}$ equality is shown by the flat curve reported in Fig. 4*A* related to the −60 mV pulse.

For depolarizing pulses positive to the I_{Ca} threshold I_{Ca} activation and deactivation are affected by inactivation and recovery from inactivation processes, respectively. To simplify the mathematical approach and the evaluation of results we assumed that for short pulse durations up to 50 ms, the time course of 'on' and 'off' currents could be considered only due to activation and deactivation since I_{Ca} inactivation and recovery from inactivation are slow phenomena with time constants in the order of seconds (cf. Francini *et al.* 1992). Indeed, in the worst condition (−10 mV) the calculation underestimated the size of the activation components by less than 1% for 100 ms and less than 0·2% for 50 ms pulse duration.

One of eighteen experiments of this type is shown in Fig. 3, where current traces elicited in response to 10 mV pulses with 5–70 ms durations are included as examples. The relation between the sum of the time integrals of the 'on' and 'off' total currents and pulse duration is reported in Fig. 4, where plots of data from −60 to 10 mV experiments are added. The early time course of activation was evaluated by fitting eqn (A31) to these data. The fitted curves (continuous lines) approach the data (symbols) very well. To approach the data the lines must be shifted by about 2 ms, confirming the presence of the time delay, t_0, due to tubular conduction of depolarization as previously found. The t_0 values evaluated in eighteen fibres were not statistically different in the voltage range tested, but

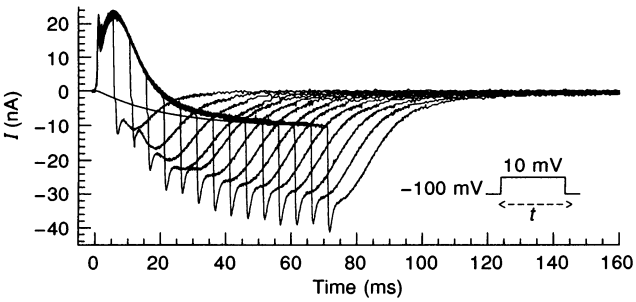

Figure 3. 'On' and 'off' currents elicited by voltage pulses of different duration

Representative current traces (test − control) evoked by voltage pulses to 10 mV from a V_h of −100 mV. Pulse duration is from 5 to 70 ms in 5 ms increments. Protocol of stimulation is shown in the inset. Continuous line is the simulation of I_{Ca} activation time course generated by eqn (A9) as a sum of three exponential functions. The amplitude parameter values were (nA): $A'P_0(V)$, −20; A_1, 0·04; A_2, 0·8 and A_3, 0·24. The time constant values were (ms): τ_1, 1; τ_2, 20; and τ_3, 260. The time delay value (t_0) was 2 ms. Values were from data calculated in Figs 2 and 4. Same fibre as Fig. 2.

seemed to decrease by increasing the depolarization; they were 2·2–2·5 ms in the range from −50 to −20 mV and 1·5–2 ms for more depolarizing pulses. The best fit was obtained by using two or three exponential functions depending on the pulse voltage. The time constant values were in the range between 5 and 180 ms and are reported in Fig. 6*C*. As expected, they agree very well with the values of the fast time constant components found with long pulse experiments (Fig. 6*A* and Table 1). The time constants slower than 200 ms were not resolved presumably due to the pulses used in this procedure being too short.

Time constants for I_{Ca} deactivation

Tail currents were determined at the end of short pulses (50–70 ms) for post-pulse potentials, 1 s long, from −120 to −50 mV in steps of 10 mV. One typical experiment is reported in Fig. 5*A*, where current traces for a post-pulse potential of −100 mV are shown as examples. Tail currents were recorded by repolarizing the membrane to post-pulse potentials after a suitable short depolarizing pulse. In skeletal muscle, tail current is the sum of two significant terms: I_{ICM} at the 'off' ($I_{ICM,off}$) and I_{Ca} deactivation ($I_{Ca,off}$). To determine the time course of $I_{Ca,off}$ we removed $I_{ICM,off}$

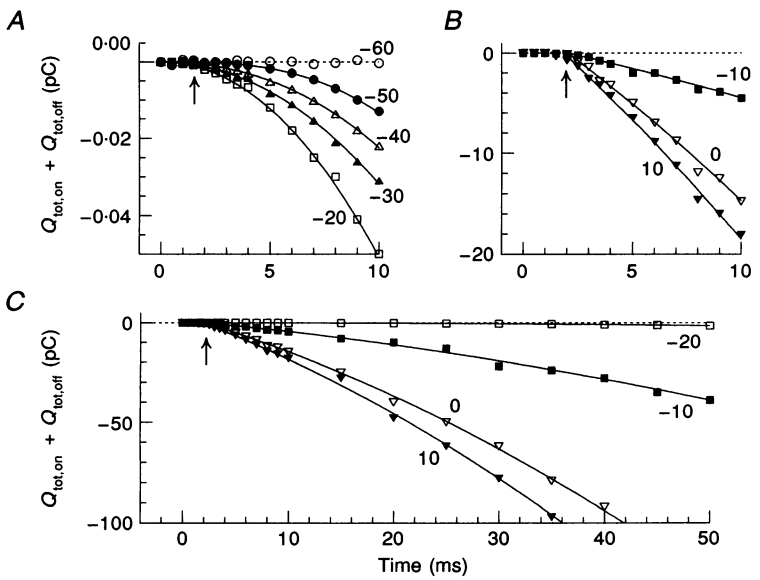

Figure 4. Evaluation of the early time course of I_{Ca}

Relation between the sum of 'on' and 'off' time integrals and time. Data are for voltage pulses from −60 to 10 mV, potentials indicated close to each curve, with durations from 0·5 to 50 ms. Continuous lines are fits of eqn (A31) to the data. For clarity, data for voltage pulses from −60 to −20 mV are reported in *A*, and from −10 to 10 mV in *B*, with different vertical scales. Time delay (t_0) is indicated by an arrow; to make it evident, only data related to pulse durations up to 10 ms are reported in *A* and *B*. Data from −20 to 10 mV related to pulse durations up to 50 ms are also reported in *C*; note the different vertical scale. Dashed lines are the zero level. Same fibre as Fig. 2; same experiment as Fig. 3.

from the total tail current with the procedure explained in the Appendix by eqns (A32) to (A34*b*). We considered that the time of relaxation of I_{ICM} at the 'on' ($I_{ICM,on}$) is voltage dependent, decreasing by increasing the depolarization. We calculated that $I_{ICM,on}$, elicited by 10 mV pulses applied from a V_h of −100 mV, is fully relaxed in less than 50 ms (cf. Fig. 2*C*). Hence, we used this voltage pulse with two different but very similar durations of 50 and 70 ms. With these parameters, the two pulses moved the same charge and the differences in amount of charge immobilization and I_{Ca} inactivation were negligible. Thus, for any given post-pulse potential, at the 'off' the time course of $I_{ICM,off}$ is similar for both pulses when they are of similar duration. With this assumption, the time course of I_{Ca} deactivation deprived of I_{ICM} was obtained by subtracting the tail current recorded following the 50 ms pulse from that recorded after the 70 ms pulse at the same voltage.

For all post-pulse potentials tested, the best fit to the time course of deactivation was obtained with a double exponential function as shown in Fig. 5*B*. Values of the two time constants determined at various post-pulse voltages are reported in Fig. 6 and means ± S.E.M. of twenty-six fibres in Fig. 8.

Voltage dependence of time constants for I_{Ca} activation

In Fig. 6*A* values of the two time constants (fast and slow) of I_{Ca} activation, evaluated in the 5 s pulse experiment of Fig. 2, are plotted on a semilogarithmic scale against voltage (filled symbols). Open symbols representing the two time constant values, fast and slow, found in deactivation (experiment of Fig. 5), are added. Fast and slow time constant values are indicated as τ_f and τ_s, respectively. The presence of two maxima, at −40 mV and at about 5 mV, is easily identified by the continuous curve superimposed on the τ_f data, confirming that at least two components are depicted in this plot. Only one maximum at −30 mV is clearly observed in the dashed curve superimposed on the τ_s data, but for potentials either negative or positive to the maximum it is easy to see that the data do not follow a single exponential function. Changes in steepness, indicated by asterisks, confirm that for this plot too there is more than a single component. These results agree with the hypothesis that at least four transitions must be assumed to explain the data. To test this possibility we fitted to each of the two groups of data (τ_f and τ_s) the following equation:

$$\sum_{i=1}^{i}\tau_i = \sum_{i=1}^{i}(k_i + k_{-i})^{-1}$$

$$= \sum_{i=1}^{i}\{\bar{K}_i[\exp(V - V_i)/k_i^* + \exp(-(V - V_i)/k_{-i}^*)]\}^{-1}, \quad (2)$$

where V is the membrane potential, V_i is the centre voltage and other parameters are defined with the same formalism of eqn (A1), taking into account that in this case they are related to the number i of apparent transitions and not to the microscopic transitions (n); the i number is arbitrary since it does not correspond to a particular position of the transition in a particular model. The best fit was obtained with $i = 2$ for τ_f as well as τ_s (continuous and dashed lines, respectively) denoting the presence of two components for

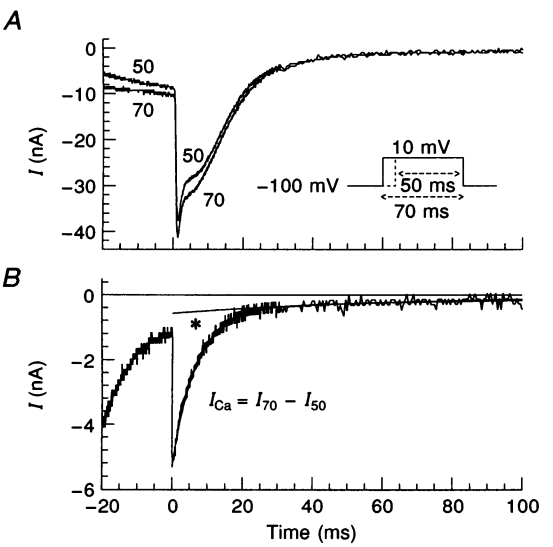

Figure 5. Time course of I_{Ca} deactivation

A, tail currents (test − control) of two 10 mV pulses lasting 50 and 70 ms; pulse protocol is shown in the inset; time zero is at the end of the pulses. *B*, the trace is the 70 ms minus the 50 ms trace of *A*. This difference represents the time course of I_{Ca} deactivation. Superimposed is the best fit of a sum of two exponential functions (time constants 6·2 and 88 ms; the mean values, calculated in twenty-six fibres, are 6 ± 0·3 and 90 ± 7 ms). Continuous line, indicated by an asterisk, is the fit of the slow exponential component. Horizontal line represents zero level. Same fibre as Fig. 2.

Table 1. Parameters of the four apparent time constants of the macroscopic I_{Ca} activation calculated in sixteen fibres

i	$\bar{K}_i$ (s^{-1})	V_i (mV)	k_i^* (mV)	k_{-1}^* (mV)
1	$\bar{K}_1 = 0{\cdot}70 \pm 0{\cdot}02$	$V_1 = -2{\cdot}0 \pm 0{\cdot}08$	$k_1^* = 21{\cdot}0 \pm 0{\cdot}5$	$k_{-1}^* = 32{\cdot}0 \pm 0{\cdot}5$
2	$\bar{K}_2 = 0{\cdot}88 \pm 0{\cdot}03$	$V_2 = -35{\cdot}0 \pm 0{\cdot}82$	$k_2^* = 11{\cdot}4 \pm 0{\cdot}4$	$k_{-2}^* = 7{\cdot}3 \pm 0{\cdot}2$
3	$\bar{K}_3 = 14{\cdot}00 \pm 0{\cdot}36$	$V_3 = -39{\cdot}0 \pm 0{\cdot}40$	$k_3^* = 5{\cdot}8 \pm 0{\cdot}1$	$k_{-3}^* = 26{\cdot}0 \pm 0{\cdot}4$
4	$\bar{K}_4 = 1{\cdot}70 \pm 0{\cdot}07$	$V_4 = 1{\cdot}8 \pm 0{\cdot}03$	$k_4^* = 12{\cdot}7 \pm 0{\cdot}3$	$k_{-4}^* = 10{\cdot}6 \pm 0{\cdot}3$

each of the two time constants. The means ± S.E.M. of the four sets of parameters of sixteen experiments are reported in Table 1.

It is easy to verify that τ_i, k_i and k_{-i} values, calculated by eqn (2) using parameters of Table 1, are not explained by a Hodgkin–Huxley model because it assumes that the rate constants mediating the transitions from resting to open state are multiples of only two voltage-dependent rate constants, α and β. Thus, for a four-transition scheme, resolving eqn (A16) for $n = 4$, we should have found 4α, 3α, 2α and α.

The presence of four time constants was confirmed by Fig. 6*B* and *C*. In Fig. 6*B* values of the three time constants of activation, resolved by the fitting to current traces in the

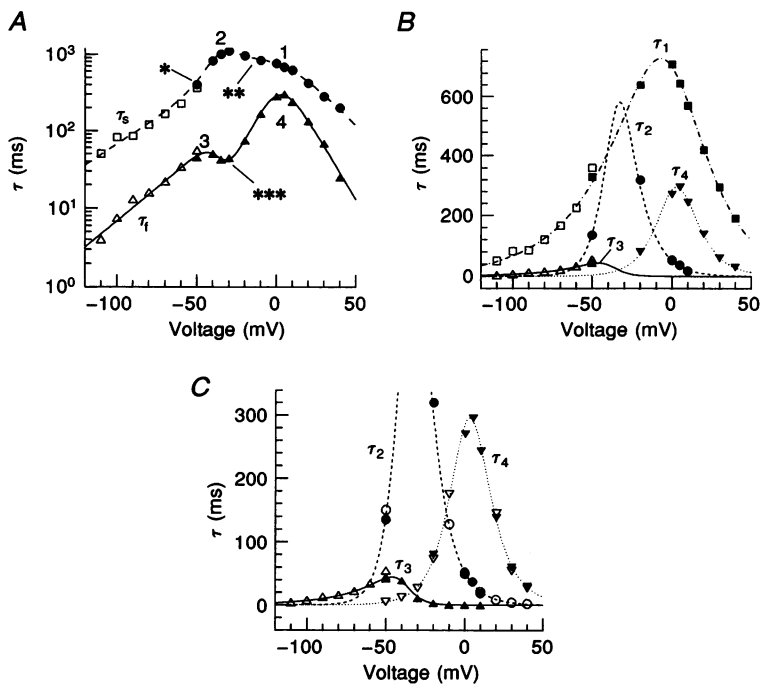

Figure 6. Voltage dependence of apparent time constants of I_{Ca} activation

A, semilogarithmic plot of fast (τ_f) and slow (τ_s) time constants of I_{Ca} activation and deactivation *vs.* voltage. The open symbols indicate τ_f (triangles) and τ_s (squares) from the I_{Ca} deactivation experiment of Fig. 5. The filled symbols indicate τ_f (triangles) and τ_s (circles) from the I_{Ca} activation experiment of Fig. 2. Curves are the fits of the sum of two terms (eqn (2)) to τ_f (continuous line) and τ_s data (interrupted line), parameters listed in Table 1. The dashed line through the points shows a clear change in steepness at −50 mV (indicated by an asterisk) and at about −10 mV (indicated by two asterisks), a clear maximum at −30 mV and a maximum-like peak near 0 mV, denoted as 2 and 1, respectively. The continuous line shows a clear minimum at −30 mV (indicated by three asterisks) and two clear maxima at −40 mV and at about 5 mV, denoted as 3 and 4, respectively. *B*, four time constants on the time course of I_{Ca}. Open symbols are the same data as in *A*. Data in the range from −50 to 10 mV (filled symbols; ●, ■ and ▼) are obtained by fitting, where possible, three exponential functions to I_{Ca} activation curves. Data in the range from 20 to 40 mV (■ and ▼) are obtained by fitting two exponential functions to the I_{Ca} activation time course. *C*, ▲, ▽ and ○ are data from the $Q_{tot,on} + Q_{tot,off}$ experiment of Fig. 4. Other symbols are from *B*, reported to make evident the presence of three time constants also in the range from 20 to 40 mV. *B* and *C*, curves are the fits of eqn (2) to four populations of data, denoted as τ_1, τ_2, τ_3 and τ_4 obtained by using the four-state cyclic model with a branch (Scheme A4 and parameters listed in Table 4).

range between −50 and 10 mV in the 5 s pulse experiment shown in Fig. 2, are plotted against voltage (filled symbols). Time constant values obtained by two-exponential fit between 20 and 40 mV (filled symbols) and deactivation time constant values (open symbols) are the same as Fig. 6*A*. In Fig. 6*C* data from the evaluation of the early time course of activation (▲, ▽ and ○) are reported. For comparison, some data from *B* (△, ● and ▼) are added. The curves reported in Fig. 6*B* and *C* are the best fits obtained by using the four-state cyclic model with a branch (Scheme A4 in the Appendix) that involves four apparent time constants (see Discussion). Curves in *B* and *C* show that data can be assembled in four groups denoted as τ_1, τ_2, τ_3 and τ_4. The same symbol, open or filled, is used for the same component to make its identification easier, the open or filled symbols are used only to identify the procedure used for its determination. Correct assignment of some data to one group was confirmed by the goodness of the fit. Comparing *B* with *C* in Fig. 6 it is clear that at extreme negative (more negative than −70 mV) and positive (more positive than 10 mV) voltages only two components can be identified, the others being very fast. At some voltages only two components can be resolved by the fitting procedure because some of them had a similar time constant value. For example, at −40 and −30 mV the component named τ_1 is similar in value to τ_2 and τ_3 to τ_4, and at −10 mV τ_2 is similar to τ_4.

Steady-state I_{Ca} activation

Typical *I–V* relations for I_{Ca} related to peak size (I_p) and to the steady-state value (I_O) determined by removing inactivation are reported in Fig. 7*A*. Data are from experiments in Fig. 2*A* and *B*, respectively.

To determine the steady-state I_{Ca} activation curve, the Goldman–Hodgkin–Katz constant-field equation, eqn (A11), was fitted to I_O data. To this aim for the steady-state open probability $P_O(V)$ we used either the general model (eqn (A8*b*)) or the m^n formalism of the Hodgkin–Huxley model (eqn (A15)). The parameters found with the two models for the amplitude factor A' of the Goldman–Hodgkin–Katz constant-field equation (eqn (A11)) were, respectively: 1·8 ± 0·2 and 1·7 ± 0·2 mM for the external Ca^{2+} activity, 150 ± 10 and 155 ± 10 mV for the reversal potential (Fig. 7*B*) and (1·78 ± 0·3) × 10^{-4} and (1·82 ± 0·027) × 10^{-4} cm s^{-1} for the limiting Ca^{2+} permeability ($n = 32$). No parameters were statistically different. The best fits were obtained using m^3 for the Hodgkin–Huxley model and four transitions for the general model. Both models were statistically less significant when less or more terms were used. Moreover, the four-transition general model improved the fit with statistical significance ($P < 0·01$) compared with the m^3 model.

The steady-state I_{Ca} activation curve (Fig. 7*C*) was obtained by dividing data points (●, of *A*) by *A'*, whose parameters

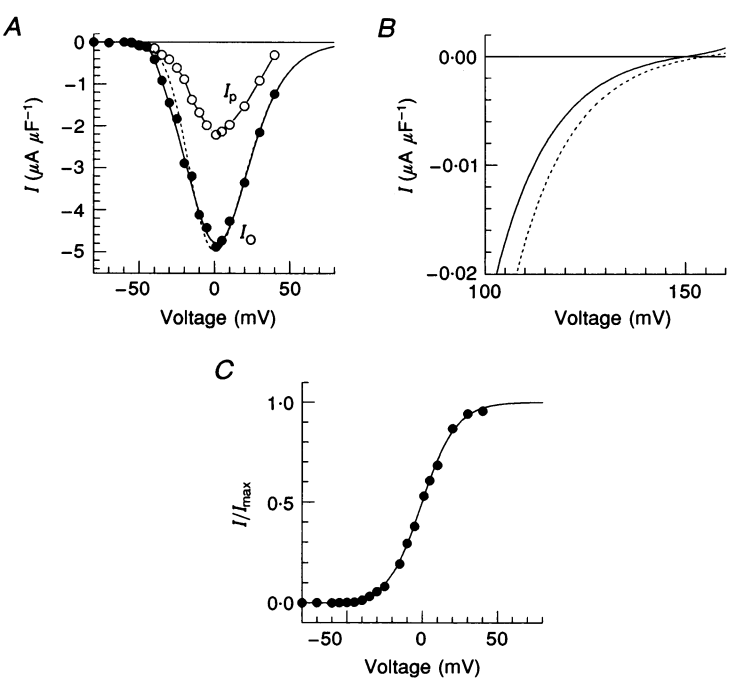

Figure 7. *I–V* curve and steady-state I_{Ca} activation curve

A, *I–V* activation curve related to I_{Ca} peak (I_p, ○) and to steady-state values determined after removing inactivation (I_O, ●). Data are from Fig. 2 and normalized to the apparent linear capacitance. Curves on I_O are fits obtained by eqn (A11) using the general model with four transitions (continuous line) or the m^3 Hodgkin–Huxley model (dashed line). *B*, detail of panel *A* demonstrating the reversal potential. *C*, normalized steady-state I_{Ca} activation data points calculated by dividing the values of I_O by *A'*, whose parameters were related to the general model with four transitions (parameters listed in Table 2). Continuous line is the best fit obtained by using this model.

Table 2. Microscopic parameters of steady-state I_{Ca} activation calculated in thirty-two fibres

E_n	k''_n (mV)	V_n (mV)
E_1	$k''_1 = 23{\cdot}0 \pm 0{\cdot}2$	$V_1 = -2 \pm 0{\cdot}2$
E_2	$k''_2 = 8{\cdot}0 \pm 0{\cdot}5$	$V_2 = -35 \pm 0{\cdot}8$
E_3	$k''_3 = 8{\cdot}5 \pm 0{\cdot}3$	$V_3 = -37 \pm 0{\cdot}3$
E_4	$k''_4 = 11{\cdot}3 \pm 0{\cdot}5$	$V_4 = 0 \pm 0{\cdot}4$

Parameters are related to the general model with four independent transitions.

were related to the four-transition general model. Since the best fit from statistical analysis as well as visual inspection (cf. Fig. 7*A*) was obtained by the four-transition model, only the parameters of this model are reported in Table 2. This result gave the values of the microscopic transitions involved in the activation pathway. However, in regard to their allocation, it indicated only the last transition before the open state (E_x in eqn (A8*b*)), whereas it did not give any indication about the others. k''_1, k''_2, k''_3 and k''_4, from $RT/F \approx 25$ (F, R and T are the usual thermodynamic constants), correspond to equivalent gating charges of 1·1, 3·1, 2·9 and 2·2, respectively. Thus, possible models are either a sequential model with four transitions or a cyclic model with five transitions, as explained in Discussion.

DISCUSSION

The present results clearly show that the activation pathway is a multistep process. The voltage dependence of the time constants found by multiexponential fit to the time course of macroscopic activation is well reproduced by at least four apparent transitions (Fig. 6). In agreement, the best simulation of the steady-state activation curve is given by assuming four microscopic independent transitions (Fig. 7*C*).

Four time-dependent exponential terms for the time course of macroscopic activation and four voltage-dependent exponential terms for steady-state activation may be explained by a different number of transitions depending on the scheme used to account for the results (see Appendix). Our results clearly demonstrate that models involving fixed rate constants such as the Hodgkin–Huxley model and the allosteric model, as in the form presented by Marks & Jones (1992), are not suitable to describe I_{Ca} activation. Thus, we analysed models with no fixed rate constants. We considered a sequential scheme as well as more complex networks.

Sequential scheme for I_{Ca} activation

To explain our results a sequential scheme must have five states and four transitions (Scheme A1). The rationale for the choice of model parameters and the allocation of the transitions for such a model are summarized in the Appendix.

The allocation of the transitions in Scheme A1 corresponds in number to that of Table 2. The microscopic parameters for each transition were calculated by solving four equations of equilibrium constants (K_n, eqn (A2*a*)) using the parameters of E_n reported in Table 2 and the four eigenvalues of the coefficient matrix obtained from the solutions of the characteristic polynomial. The E_n parameters, τ_i and A_i data (Fig. 8), obtained in the same fibres, were used for calculation. The real A_i values were not resolved by tail current analysis, but eqn (A34) allowed estimation of their relative values. Following this, parameters were slightly adjusted until simulated data generated from the model

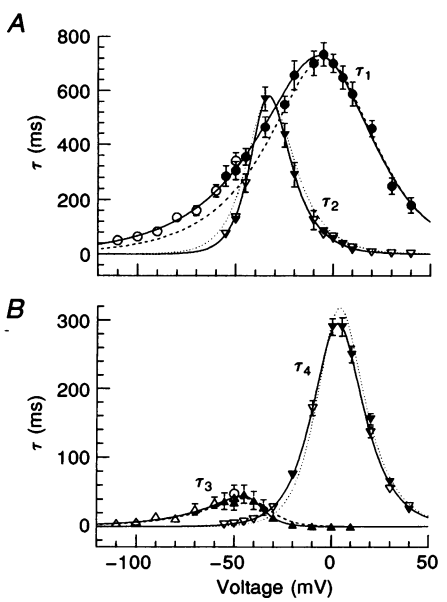

Figure 8. Comparison of fits of the five-state sequential model and four-state cyclic model with a branch

Voltage dependence of the four apparent time constants of activation. For clarity, τ_1 and τ_2 are reported in *A* and τ_3 and τ_4 in *B* with a different ordinate scale. *A*: τ_1, open and filled circles are from deactivation and activation experiments, respectively; τ_2, open and filled triangles are from $Q_{tot,on} + Q_{tot,off}$ and activation experiments, respectively. *B*: τ_3, open and filled triangles are from deactivation and $Q_{tot,on} + Q_{tot,off}$ experiments, respectively; open circle is from activation experiments. τ_4, open and filled triangles are from $Q_{tot,on} + Q_{tot,off}$ and activation experiments, respectively. Data points represent mean values from 45 fibres. Each data point is from 8 to 32 experiments. Error bars are shown when the S.E.M. exceeded the symbol size. The interrupted lines show the prediction of the five-state sequential model. This model was unable to account for the potential dependence of all the four time constants. The prediction from the four-state cyclic model with a branch is shown by the continuous lines, which indicate that this model was able to describe the voltage dependence of the apparent time constants for I_{Ca} activation accurately over the potential range tested.

Depolarized

$$\underset{}{} \quad \tau_1 = 509 \qquad \tau_2 = 9{\cdot}1 \qquad \tau_3 = 0{\cdot}27 \qquad \tau_4 = 141$$

$$S_1(R) \longrightarrow S_2 \longrightarrow S_3 \longrightarrow S_4 \longrightarrow S_5(O)$$

$$(\tau_{-1} = 1{\cdot}3 \times 10^3) \quad (\tau_{-2} = 8{\cdot}8 \times 10^3) \quad (\tau_{-3} = 221) \quad (\tau_{-4} = 831)$$

Repolarized

$$(\tau_1 = 4{\cdot}8 \times 10^3) \quad (\tau_2 = 400) \quad (\tau_3 = 1 \times 10^4) \quad (\tau_4 = 2{\cdot}8 \times 10^3)$$

$$S_1(R) \longleftarrow S_2 \longleftarrow S_3 \longleftarrow S_4 \longleftarrow S_5(O)$$

$$\tau_{-1} = 66{\cdot}4 \qquad \tau_{-2} = 0{\cdot}12 \qquad \tau_{-3} = 6{\cdot}8 \qquad \tau_{-4} = 0{\cdot}4$$

Scheme 1

adequately fitted the experimental results. The parameters that gave the best simulation are reported in Table 3 and the simulated τ_i *vs.* voltage relation in Fig. 8 (interrupted lines). The time constant values ($\tau_n = 1/k_n$ and $\tau_{-n} = 1/k_{-n}$, where k_n and k_{-n} are from eqn (A1) using parameters of Table 3), in milliseconds, occurring after changing the membrane potential from a V_h of −100 to 20 mV ('Depolarized') and vice versa ('Repolarized'), are reported in Scheme 1, where arrows denote the direction of the transition during depolarization or repolarization. The slower time constant values in the opposite direction are reported in parentheses.

Cyclic schemes for I_{Ca} activation

More complex networks that include loops were considered. For each loop the condition of microscopic reversibility must be satisfied (eqn (A4)).

A model with one four-state loop with a branch was found suitable to describe the experimental data. It involved five transitions one of which was dependent on the others (Scheme A4). The rationale for the choice of model parameters and the allocation of the transitions for such a model are summarized in the Appendix.

The calculation related to the choice of the microscopic parameters followed the procedure and considerations reported for the sequential scheme, taking into account the eigenvalues of the coefficient matrix obtained resolving the characteristic polynomial for the model of Scheme A4. The numerical values that gave the best simulation of data are reported in Table 4. The time constant values (τ_n), in milliseconds, occurring after changing the membrane potential from a V_h of −100 mV to 20 mV ('Depolarized') and vice versa ('Repolarized'), are reported in Scheme 2 and the simulated τ_i *vs.* voltage relation in Fig. 8 (continuous lines).

Both Schemes 1 and 2 appear formally equivalent to describe the presence of two time constants of the macroscopic I_{Ca} activation on depolarization and two time constants on repolarization. But these two schemes show some differences.

For the sequential scheme, after repolarization, state S_2 is relatively stable allowing fast opening (via $S_2 \rightarrow S_3 \rightarrow S_4 \rightarrow S_5$ (O)) on a second depolarization. For the cyclic scheme there are two relatively stable states (S_2 and S_4) allowing fast opening (via $S_2 \rightarrow S_3$ and $S_4 \rightarrow S_3$) on a second depolarization. Therefore, the opening requires the action of both mechanisms in conjunction. A comparison of the fits of the five-state sequential (interrupted lines) and four-state cyclic with a branch (continuous lines) models to averaged time constant values from forty-five fibres, is shown in Fig. 8. The sequential model was unable to adequately account for the voltage dependence of all τ_i, particularly for τ_1 at negative potentials. In contrast, the cyclic model was able to account for the data accurately over the voltage range tested. Moreover, the fit was statistically more significant for the four-state cyclic with a branch model than for the five-state sequential model: F statistics for the fitted curves related to τ_1, τ_2, τ_3 and τ_4 *vs.* voltage (Fig. 8) gave $F > 0{\cdot}9995$ and $0{\cdot}99 < F < 0{\cdot}999$, respectively; P values from Student's t test related to each individual parameter were $P < 0{\cdot}001$ and $0{\cdot}5 < P < 0{\cdot}01$, respectively.

From Table 4, k_1'', k_2'', k_3'', k_4'' and k_o'', being $RT/F \approx 25$, correspond to equivalent gating charges of 3·1, 2·9, 5, 1·1 and 2·2. On depolarization the cyclic model has the first two transitions from the resting state, $S_1(R) \rightarrow S_2$ and $S_1(R) \rightarrow S_4$, that are rate limiting and move 3·1 and 1·1 charges, respectively. Both are followed by fast transitions $S_2 \rightarrow S_3$ and $S_4 \rightarrow S_3$ that move 2·9 and 5 charges, respectively. Hence, both branches of the loop move about six charges towards S_3. Finally, the last step, $S_3 \rightarrow S_5$(O), is slow and high-voltage activated, and leads to calcium channel opening moving two other charges. For the different voltage dependence of the two transitions of each branch (Table 4) the $S_3 \rightarrow S_4 \rightarrow S_1(R)$ pathway is favoured on repolarization. In contrast, on depolarization, beyond about −35 mV, the favoured branch is $S_1(R) \rightarrow S_2 \rightarrow S_3$, being the half-voltage value of each transition at negative

Table 3. Microscopic parameters of the four transitions for the five-state sequential model for I_{Ca} activation calculated in forty-five fibres

E_n	k''_n (mV)	$\bar{K}_n$ (s^{-1})	V_n (mV)	k^*_n (mV)	k^*_{-n} (mV)
E_1	$k''_1 = 23{\cdot}0 \pm 2{\cdot}1$	$\bar{K}_1 = 1{\cdot}3 \pm 0{\cdot}3$	$V_1 = -2 \pm 0{\cdot}2$	$k^*_1 = 53{\cdot}4 \pm 4{\cdot}4$	$k^*_{-1} = 40{\cdot}0 \pm 2{\cdot}2$
E_2	$k''_2 = 8{\cdot}0 \pm 1{\cdot}5$	$\bar{K}_2 = 19{\cdot}4 \pm 2{\cdot}2$	$V_2 = -35 \pm 1{\cdot}8$	$k^*_2 = 31{\cdot}7 \pm 2{\cdot}5$	$k^*_{-2} = 10{\cdot}7 \pm 1{\cdot}5$
E_3	$k''_3 = 8{\cdot}5 \pm 0{\cdot}8$	$\bar{K}_3 = 23{\cdot}6 \pm 1{\cdot}7$	$V_3 = -37 \pm 1{\cdot}3$	$k^*_3 = 11{\cdot}3 \pm 1{\cdot}8$	$k^*_{-3} = 34{\cdot}5 \pm 2{\cdot}3$
E_4	$k''_4 = 11{\cdot}3 \pm 1{\cdot}1$	$\bar{K}_4 = 4{\cdot}3 \pm 0{\cdot}6$	$V_4 = 0 \pm 0{\cdot}4$	$k^*_4 = 40{\cdot}1 \pm 3{\cdot}1$	$k^*_{-4} = 15{\cdot}7 \pm 2{\cdot}4$

Table 4. Microscopic parameters of the five transitions for the four-state cyclic model with a branch for I_{Ca} activation calculated in forty-five fibres

E_n	k''_n (mV)	$\bar{K}_n$ (s^{-1})	V_n (mV)	k^*_n (mV)	k^*_{-n} (mV)
E_1	$k''_1 = 8{\cdot}0 \pm 2{\cdot}1$	$\bar{K}_1 = 0{\cdot}06 \pm 1 \times 10^{-4}$	$V_1 = -35 \pm 1{\cdot}8$	$k^*_1 = 19{\cdot}0 \pm 1{\cdot}1$	$k^*_{-1} = 13{\cdot}8 \pm 1{\cdot}0$
E_2	$k''_2 = 8{\cdot}5 \pm 1{\cdot}5$	$\bar{K}_2 = 23{\cdot}7 \pm 1{\cdot}4$	$V_2 = -37 \pm 1{\cdot}3$	$k^*_2 = 11{\cdot}5 \pm 0{\cdot}9$	$k^*_{-2} = 32{\cdot}4 \pm 1{\cdot}7$
E_3	$k''_3 = 5{\cdot}0 \pm 0{\cdot}8$	$\bar{K}_3 = 0{\cdot}24 \pm 1{\cdot}1$	$V_3 = -44 \pm 0{\cdot}8$	$k^*_3 = 10{\cdot}8 \pm 0{\cdot}8$	$k^*_{-3} = 9{\cdot}4 \pm 0{\cdot}6$
E_4	$k''_4 = 23{\cdot}0 \pm 1{\cdot}1$	$\bar{K}_4 = 1{\cdot}7 \pm 0{\cdot}2$	$V_4 = -2{\cdot}0 \pm 0{\cdot}2$	$k^*_4 = 32{\cdot}9 \pm 1{\cdot}7$	$k^*_{-4} = 52{\cdot}5 \pm 2{\cdot}6$
E_O	$k''_O = 11{\cdot}3 \pm 1{\cdot}4$	$\bar{K}_O = 4{\cdot}7 \pm 0{\cdot}4$	$V_O = 0{\cdot}0 \pm 0{\cdot}4$	$k^*_O = 30{\cdot}6 \pm 1{\cdot}5$	$k^*_{-O} = 17{\cdot}9 \pm 1{\cdot}1$

potential ($V_1 = -35$ mV and $V_2 = -37$ mV), whereas the other branch has one transition activated at high voltage ($V_4 = -2$ mV).

Early fast steps on repolarization followed by slow step(s) are necessary to explain, in double-pulse experiments, the quicker activation and the potentiation of current traces during the second depolarization (Feldmeyer *et al.* 1990; García, Avila-Sakar & Stefani, 1990; Francini *et al.* 1992). These were tentatively explained by the fast kinetics on repolarization of the last transition $O \rightarrow C_2$ and the slow kinetics of the transition $C_2 \rightarrow C_1$ leading to the resting state C_1 for the sequential model proposed in Scheme 1 by Francini *et al.* (1992), or by the fast $O \rightarrow C_4$ and slow

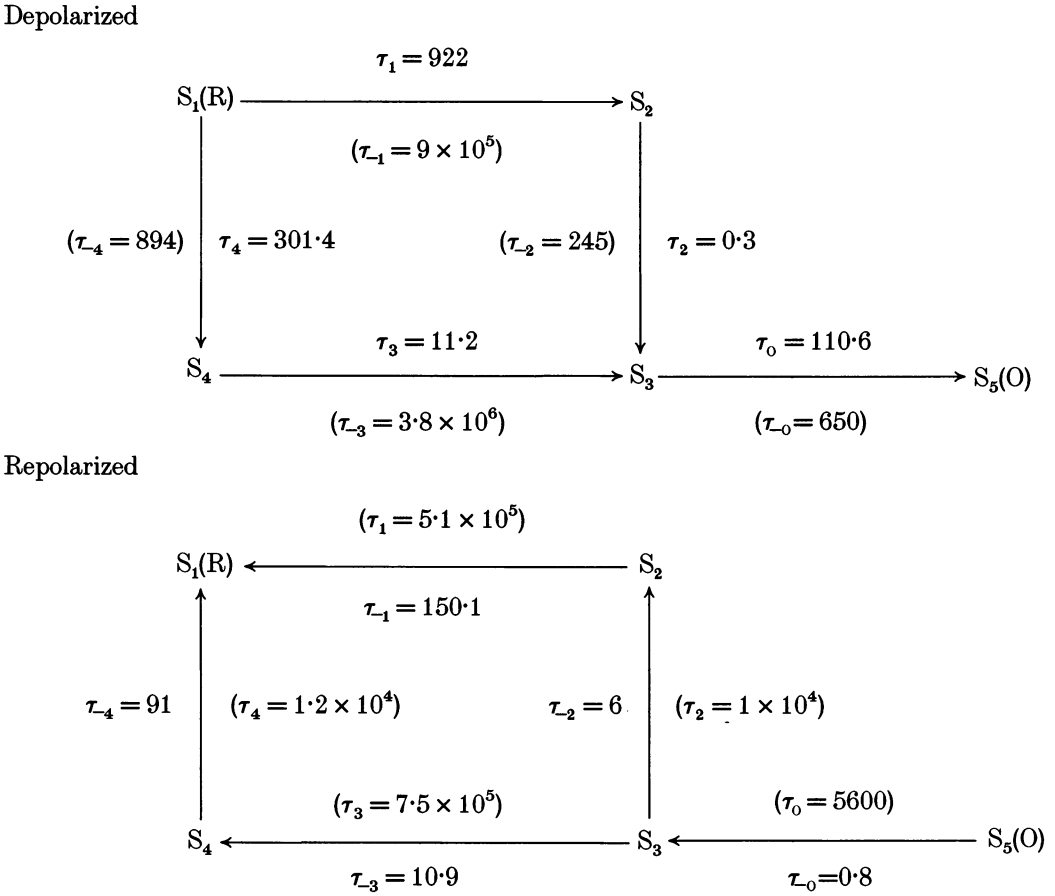

Scheme 2

$C_4 \rightarrow C_1$ transition of the cyclic model proposed in Fig. 8 by Feldmeyer *et al.* (1990). In the present work this phenomenon is explained by the fast transitions of $S_5(O) \rightarrow S_4 \rightarrow S_3 \rightarrow S_2$ and the slow transition $S_2 \rightarrow S_1(R)$ of the sequential model (Scheme 1). In the four states with a branch model (Scheme 2), there is a fast closing $S_5(O) \rightarrow S_3$ followed by two relatively fast transitions $S_3 \rightarrow S_2$ and $S_3 \rightarrow S_4$, both slowly leading to the resting state. Feldmeyer and co-workers (Feldmeyer *et al.* 1990, 1995; Feldmeyer, Melzer, Pohl & Zöllner, 1992) described their results using a four-state model such as Scheme A2 only in qualitative terms. This model did not fit our results because from eqn (A14*c*) it involved only three apparent time constants.

Dihydropyridine binding sites and calcium channels

Schwartz *et al.* (1985) proposed that there are 35–50 times more DHP binding sites than functional or activatable calcium channels. This could indicate that only a few of the DHP receptors are in fact Ca^{2+} channels which exhibit open-state probability at large depolarizations while the vast majority are structurally different and never open. Another possibility could be that all DHP receptors are structurally identical Ca^{2+} channel molecules which, however, exhibit a very small open-state probability even at large depolarizations.

Our results reported that at 0 mV only about 50% ($P_O = 0{\cdot}45 \pm 0{\cdot}02$, $n = 32$) of Ca^{2+} channels are in the open state (cf. Fig. 7*C*). A full activation may be obtained by very strong depolarization (above 50 mV). The discrepancy with other previous results reporting a full activation and/or half-voltage value of L-type Ca^{2+} channels towards more negative potentials (Almers & Palade, 1981; Sánchez & Stefani, 1983; for a review see McDonald *et al.* 1994) could be due to many reasons: (1) a short examination of the 'off' tail current that considered only the early decay or assumed that the tail current decayed with a single exponential function; these types of evaluation underestimate the size of I_{Ca} deactivation by about 30–40%; (2) I_{ICM} contamination was considered negligible with respect to the I_{Ca} tail; present results, with 2 mM extracellular Ca^{2+} concentration, show a 20–50% of contamination that significantly affected the evaluation of the steady-state activation curve; (3) acquisition of data was made in a narrow voltage range not including strong positive potentials, thus extrapolation of the fit from these fractional data could be misleading.

The present work shows that the presence of inactivation significantly reduced the steady-state evaluation of I_{Ca}. Indeed, the removal of inactivation showed that I_{Ca} peak current at 0 mV was about 25–35% of the true value (cf. Fig. 7*A*). Hence, the recorded peak current of $2{\cdot}4 \pm 0{\cdot}2$ $\mu A\ \mu F^{-1}$ per unit of linear capacitance (mean membrane capacitance, $6{\cdot}56 \pm 0{\cdot}3$ nF) or $7{\cdot}96 \pm 0{\cdot}3$ mA ml^{-1} per unit of fibre volume (fibre diameter, 80 ± 5 μm; $n = 32$) corresponded after removing inactivation, to a true current of $7{\cdot}2 \pm 0{\cdot}4$ $\mu A\ \mu F^{-1}$ or $23{\cdot}88 \pm 0{\cdot}7$ mA ml^{-1}.

According to Lamb & Walsh (1987), to evaluate whether all DHP receptors are also activatable L-type Ca^{2+} channels, or not, we must consider whether: (1) the average fraction of time that a channel is open (P) is < 1; indeed, at 0 mV it is only 0·05–0·25 in absence of agonists (Coronado & Affolter, 1986; Flockerzi, Oeken, Hofmann, Pelzer, Cavalié & Trautwein, 1986); and (2) the number of DHP binding sites per channel may be four (one for each unit of the tetrad) or, according to Lamb & Walsh (1987), 1·5–3.

In six experiments with 10 mM external Ca^{2+} concentration, the peak current at 0 mV increased 3·4 times while P_O decreased from 0·45 to 0·3, because of a 10 mV shift to more positive potentials due to the raised Ca^{2+} concentration. The I_{Ca} peak current value was $8{\cdot}3$ $\mu A\ \mu F^{-1}$ or 27 mA ml^{-1}. Assuming $P = 0{\cdot}08$, 5×10^{13} DHP binding sites per millilitre fibre volume (Schwartz *et al.* 1985) and three DHP binding sites per channel, the calculated single-channel current amplitude is 0·23 pA. This value is compatible with estimates reported in previous works ranging from 0·1 to 0·5 (Hess & Tsien, 1984; Mejía-Alvarez, Fill & Stefani, 1991; Dirksen & Beam, 1995). Therefore, we conclude that in skeletal muscle of the frog most of the DHP receptors are also activatable L-type Ca^{2+} channels.

Consequently, the DHP receptor has a dual function: (1) as a sensor for EC coupling; the model of Scheme 2 can explain the rapid activation of an SR Ca^{2+}-release channel if the coupling with the ryanodine receptor lies in S_3. Indeed, the calculated overall time constant for S_3 mobilization was about 20 ms at 20 mV, rapid enough to account for activation of SR Ca^{2+} release (Ríos & Pizarro, 1991; Ríos *et al.* 1993); and (2) as a Ca^{2+} channel its activation induces a Ca^{2+} input flux that in particular conditions, such as during repetitive (tetanic) stimulation, may act on the opposite Ca^{2+}-release channel (foot) triggering a calcium-induced calcium release (Meissner, 1994).

APPENDIX

Models for I_{Ca} activation

Rate theory models. Taking into account the different types of schemes for I_{Ca} activation reported in the literature, various sets of calculations have been performed to find the best model matching our experimental findings. The behaviour of the models was determined using the Q matrix formalism of Colquhoun & Hawkes (1977). The parameters describing the time course of the open probability were derived from the eigenvalues and eigenvectors of the Q matrix. The justification for all the assumptions and analysis are only outlined, principally to define and state particular schemes discussed here (for more details about sequential models see Taylor, 1988).

From a topological point of view one- and two-transition models can only be described by sequential schemes, but if a model has three or more transitions it may be either

sequential or cyclic. For example, a four-transition sequential model is presented in Scheme A1,

$$S_1(R) \underset{k_{-1}}{\overset{k_1}{\rightleftharpoons}} S_2 \underset{k_{-2}}{\overset{k_2}{\rightleftharpoons}} S_3 \underset{k_{-3}}{\overset{k_3}{\rightleftharpoons}} S_4 \underset{k_{-4}}{\overset{k_4}{\rightleftharpoons}} S_5(O)$$

Scheme A1

and a four-transition cyclic model in Scheme A2,

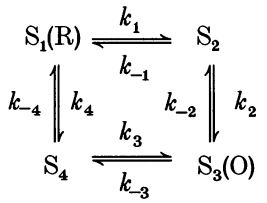

Scheme A2

where R indicates the resting state and O the activated–open state. All other states are activated–closed. Each transition in the kinetic schemes has two microscopic rate constants associated with it: k_n and k_{-n}. In agreement with conventional rate theory, we assume exponential dependence of rate constants on voltage:

$$k_n = \bar{K}_n \exp[(V - V_n)/k^*_n],$$
$$k_{-n} = \bar{K}_n \exp[-(V - V_n)/k^*_{-n}], \quad \text{(A1)}$$

where n denotes the rate constants always defined in the direction from resting (R) to open state (O), and $-n$ in the reverse direction, $\bar{K}_n$ is the voltage-independent value at the centre voltage (V_n), V is the membrane potential, $k^*_n = RT/z_nF$, $k^*_{-n} = RT/z_{-n}F$ and z is the equivalent charge moved across the membrane electric field in the forward or backward direction.

The equilibrium constants (K_n), always defined in the direction from the resting to the open state, are:

$$K_n = k_n/k_{-n} = \exp[(V - V_n)/k''_n]. \quad \text{(A2}a\text{)}$$

In this equation $k''_n = RT/Z_nF$, where Z_n is the magnitude of the equivalent electronic charge which moves across the membrane electric field in the transition.

For convenience in the simulation and calculation we will use the dissociation constant:

$$E_n = 1/K_n. \quad \text{(A2}b\text{)}$$

For any scheme there is the conservation condition that the probabilities of occupancy (P_j) of each state (S_j) add to the unit:

$$P_1 + \ldots + P_j = \sum_{j=1}^{j} P_j = 1. \quad \text{(A3)}$$

For a single-cycle model there is also an equation of microscopic reversibility:

$$E_1E_2 = E_3E_4. \quad \text{(A4)}$$

The steady-state probability, $P_O(V)$, of being $S_j(O)$ in the activated–open state, can be obtained as a function of voltage by sequential substitutions between eqns (A2) and (A3).

For a general sequential scheme:

$$P_O(V) = 1/(1 + E_n + E_nE_{n-1} + E_nE_{n-1}E_{n-2} + \ldots + E_n \ldots E_1). \quad \text{(A5}a\text{)}$$

In the example of Scheme A1:

$$P_O(V) = 1/(1 + E_4 + E_4E_3 + E_4E_3E_2 + E_4E_3E_2E_1). \quad \text{(A5}b\text{)}$$

In a single-cycle model as Scheme A2 we have:

$$P_O(V) = 1/(1 + E_2 + E_2E_1 + E_2E_1E_4^{-1}). \quad \text{(A6)}$$

Equation (A6) shows that in the single-cycle model one factor (E_3) is not expressed but is defined by the others; it can be calculated from eqn (A4):

$$E_3 = E_1E_2E_4^{-1}. \quad \text{(A7)}$$

For any network of x states, $P_O(V)$ can be written in the general form:

$$P_O(V) = 1/(1 + E_x + E_xE_{x-1} + E_xE_{x-1}E_{x-2} + \ldots + E_x \ldots E_1), \quad \text{(A8}a\text{)}$$

where x is an arbitrary number without any relation to the allocation of each transition in a kinetic pathway. Equation (A8a) only assesses that the last transition before the open state has the microscopic parameter E_x. To make the fitting procedure easier eqn (A8a) can be simplified by writing it in the following form:

$$P_O(V) = 1/(1 + E_A + E_B + \ldots), \quad \text{(A8}b\text{)}$$

where $E_A = E_x$, $E_B = E_xE_{x-1}$ and so on up to the product of x factors.

Time course of I_{Ca} activation. For any network of states, the time course of I_{Ca} activation as a function of membrane potential and time is expressed in a general form by:

$$I_{Ca,O}(V,t) = A'P_O(V)P_O(t), \quad \text{(A9)}$$

where $P_O(t)$ is the time-dependent probability of being S_j in the activated–open state that can be expressed as a sum of exponential terms,

$$P_O(t) = 1 - \{\bar{A}_1 \exp[-(t - t_0)/\tau_1] + \ldots + \bar{A}_i \exp[-(t - t_0)/\tau_i]\}$$
$$= 1 - \sum_{i=1}^{i} \bar{A}_i \exp[-(t - t_0)/\tau_i], \quad \text{(A10)}$$

where i is the number of time-dependent terms of the macroscopic current, with the time constant τ_i and $\bar{A}_i$ being the related amplitude factors; both τ_i and $\bar{A}_i$ are functions of microscopic rate constants and are given by the eigenvalues and eigenvectors of the coefficient matrix (see Taylor, 1988); the time t_0 is introduced to account for the presence of a possible time delay due to the tubular system (Huang & Peachey, 1992).

The steady-state activation curve is given by:

$$I_{Ca}(V) = A' P_O(V), \quad \text{(A11)}$$

that represents the Goldman–Hodgkin–Katz constant-field equation (Meves & Vogel, 1973; Sánchez & Stefani, 1983), where A' is:

$$A' = (\bar{P}_{Ca} Z^2 VF^2/RT) a_o \times \{\exp[Z(V - V_{Ca})F/RT] - 1\}/[\exp(ZVF/RT) - 1], \quad \text{(A12}a\text{)}$$

where a_o is the activity of calcium outside, $\bar{P}_{Ca}$ is the limiting Ca^{2+} permeability, Z is the valency and V_{Ca} is the reversal potential. It follows that the voltage dependence of Ca^{2+} permeability is:

$$P_{Ca} = \bar{P}_{Ca} P_O(V). \quad \text{(A12}b\text{)}$$

Since the ionic current must be zero at time equal to zero, eqn (A10) must satisfy the condition:

$$\bar{A}_{tot} = \sum_{i=1}^{i} \bar{A}_i = 1. \quad \text{(A13)}$$

The relations between the number (i) of the time-dependent terms of the macroscopic current (eqn (A10)) and the number (n) of transitions, and between n and the number (j) of states (S_j), depend on the model type. They are: in sequential schemes,

$$n = i \text{ and } j = n + 1; \quad \text{(A14}a\text{)}$$

and in multiple-cycle schemes, as allosteric models,

$$n = i + L \text{ and } j = n - L + 1, \quad \text{(A14}b\text{)}$$

where L is the number of loops; in the special case of a single loop,

$$n = i + 1 \text{ and } j = n. \quad \text{(A14}c\text{)}$$

It is interesting to note, by comparing eqns (A14a) and (A14c), that the number of terms (i) in eqn (A10) is equal to n in sequential models but is one unit less than the number of transitions in a single-cycle model. The relation $j = i + 1$ is true for every model.

Models with fixed rate constants. A short description of two particular models, the Hodgkin–Huxley and allosteric models, used to simulate voltage-dependent channels, follows.

In the Hodgkin–Huxley model, activation gates are assumed to be completely independent. That is, each gate can open and close regardless of the condition of the other gates. In this model the kinetics are fully defined by only two parameters, α and β, corresponding to k_1 and k_{-1} of eqn (A1). The steady-state open probability (cf. eqn (A5)) may be expressed in a simple form as:

$$P_O(V) = m^n = 1/(1 + E_1)^n, \quad \text{(A15)}$$

and the time course of current activation (cf. eqn (A10)) as:

$$P_O(t) = \{1 - \exp[-(t - t_0)/\tau]\}^n, \quad \text{(A16)}$$

where m^n corresponds to the usual notation for the Hodgkin–Huxley model and n is the number of transitions in the activation pathway, $E_1 = \beta/\alpha$, $\tau = 1/(\alpha + \beta)$. From eqn (A14$a$) or resolving eqn (A16), it is easy to verify that $n = i$. In the original Hodgkin–Huxley model it was $n = 3$ and the ratio of forward and backward rate constants was $3\alpha : 2\alpha : 1\alpha$ and $1\beta : 2\beta : 3\beta$, respectively.

The allosteric model for channel activation assumes multiple closed and open states and its kinetics are fully defined by only five parameters. It is described by multiple cyclic interactions with voltage-dependent transitions between the closed states as well as between the open states, both with fixed rate constants, as in the Hodgkin–Huxley model. Moreover, it has voltage-independent transitions between the closed and the open states (for involved formalisms see: Marks & Jones, 1992; Ríos *et al.* 1993).

Kinetic models for four apparent time constants of I_{Ca} activation. Since our results give clear evidence for the presence of four apparent time constants for activation we discuss some possible kinetic models.

From eqn (A14a), a sequential scheme must have five states and four transitions (Scheme A1). The rationale for the choice of model parameters and the allocation of the transitions for such a model are summarized as follows.

(1) From Fig. 6B and C it is clear that at extreme potentials only two apparent rate constants become rate limiting. Thus, the microscopic rates of activation can be determined by the two rate constants of macroscopic activation (τ_1 and τ_4) at extreme positive potentials, that is the scheme can be reduced to one having only two transitions. Similarly, the microscopic rates of deactivation were determined by the two observed rate constants of macroscopic deactivation at extreme negative potentials (τ_1 and τ_3).

(2) The observed half-voltage value of the steady-state activation curve, V_{tot}, (Fig. 7C) is at about 0 mV ($1 \pm 0{\cdot}02$, $n = 32$), so the last transition (i.e. the closed–open transition) cannot have a negative half-voltage value, V_n. In such a case, V_{tot} should have been shifted towards negative potentials. Therefore, the microscopic transitions E_2 and E_3 (Table 2) are excluded, being $V_2 = -35$ and $V_3 = -37$ mV, respectively. Moreover, both E_1 and E_4 have a V_n value near zero (−2 and 0 mV, respectively); consequently if both were set near to the open state, the total steady-state curve should show a more positive V_{tot} value. In conclusion, E_4 must be the last transition and E_1 the first with respect to the resting state, or vice versa.

(3) To observe the fast and the slow exponential decays (τ_1 and τ_3 in Fig. 6B and C) on the deactivating current, on repolarization, the transition with the slow kinetic must be allocated near to the resting state and the fast towards the open state (i.e. the open–closed transition). Therefore, from the open to the resting state E_3 must precede E_1. Thus, from point (2), E_4 must be the last transition and E_1 the first with respect to the resting state, whereas the opposite is not possible.

(4) The assignment of allocation of each transition is from eqn (A8*a*) and eqn (A5*b*), considering the correspondence of the first term of each equation (i. e. $E_{x=4}$ corresponds to E_4) and so on for the other terms. That is, the term with a single factor (E_4) is the last transition, the term as a product of two factors (E_4E_3) denotes that the previous transition is E_3 and so on. Thus, the sequence from resting to open state is E_1, E_2, E_3 and E_4.

According to eqn (A14*c*), to describe the four terms of macroscopic current and the four microscopic terms of the steady-state activation curve, a single-cycle scheme must have five states as well as five transitions, one of which with parameters determined by those of the four others. Scheme A3 represents a probable solution where the open state is allocated in S_4, but any other position is theoretically possible.

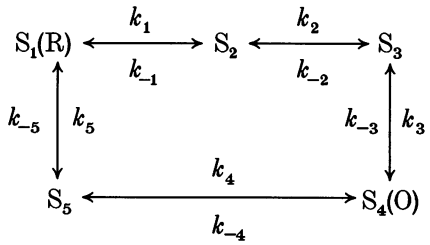

Scheme A3

Several alternatives to Scheme A3 exist as a single loop with a branch. Two possible solutions are reported as examples in Schemes A4 (four-state loop with a branch from S_3) and A5 (three-state loop with a two-transition branch from S_2).

For the loop of each model there is an equation of microscopic reversibility (eqn (A4)) for which the product of the equilibrium constants of a branch must be equal to that of the other branch. For Scheme A3 we have:

$$E_1E_2E_3 = E_4E_5. \quad \text{(A17}a\text{)}$$

Conformity with eqn (A17*a*) requires the forward flux (clockwise direction) to be equal to the backward flux (anticlockwise direction), and from this it follows that

$$k_1k_2k_3k_{-4}k_{-5} = k_{-1}k_{-2}k_{-3}k_4k_5. \quad \text{(A17}b\text{)}$$

The steady-state activation is given by:

$$P_O(V) = 1/(1 + E_3 + E_3E_2 + E_3E_2E_1 + E_3E_2E_1E_5^{-1}), \quad \text{(A17}c\text{)}$$

and from eqn (A17*a*) the E_4 is given by:

$$E_4 = E_1E_2E_3E_5^{-1}. \quad \text{(A17}d\text{)}$$

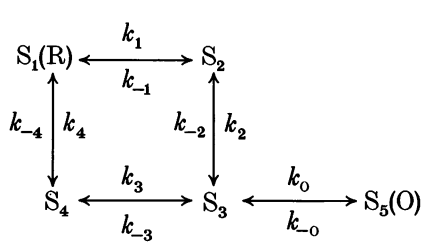

Scheme A4

For Scheme A4 the corresponding equations are:

$$E_1E_2 = E_3E_4, \quad \text{(A18}a\text{)}$$

$$k_1k_2k_{-3}k_{-4} = k_{-1}k_{-2}k_3k_4, \quad \text{(A18}b\text{)}$$

$$P_O(V) = 1/(1 + E_O + E_OE_2 + E_OE_2E_1 + E_OE_2E_1E_4^{-1}), \quad \text{(A18}c\text{)}$$

$$E_3 = E_1E_2E_4^{-1} \quad \text{(A18}d\text{)}$$

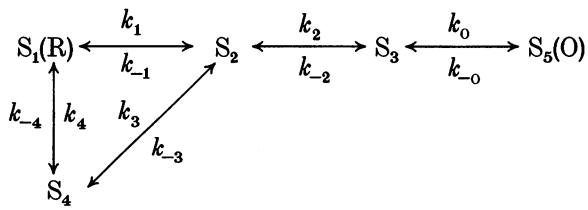

Scheme A5

For Scheme A5:

$$E_1 = E_3E_4, \quad \text{(A19}a\text{)}$$

$$k_1k_{-3}k_{-4} = k_{-1}k_3k_4, \quad \text{(A19}b\text{)}$$

$$P_O(V) = 1/(1 + E_O + E_OE_2 + E_OE_2E_1 + E_OE_2E_1E_4^{-1}), \quad \text{(A19}c\text{)}$$

$$E_3 = E_1E_4^{-1}. \quad \text{(A19}d\text{)}$$

For reasons of microscopic balance Scheme A3 does not work because eqn (A17*a*) is not verified. The same result is obtained if the allocation of the O state is changed from S_4 to S_3 or S_2. Microscopic balance is verified only if the O state is in S_5, but such a model would involve, on repolarization, an approximately 100 times quicker rate constant leading to R than that observed. Consequently, deactivation should show only a fast component because the fast transition $S_5(O) \rightarrow S_1(R)$ is favoured with respect to the slow pathway of the other branch of the loop. Moreover, the time course of activation involving mainly a single transition gives a lower lag than that observed.

In contrast, microscopic balance is satisfied for both Schemes A4 and A5. Scheme A5 simulates both fast and slow deactivating components but the fast component was about one order slower than that observed. With regard to Scheme A4 other allocations of the branch leading to O as in $S_1(R)$, S_2 or S_4 do not satisfy the conditions of microscopic balance. Consequently, with respect to cyclic models, only Scheme A4 is suitable to describe the experimental data.

The numerical values that gave the best simulation of data are reported in Table 4.

Mathematical dissection of data

Evaluation of time course of I_{Ca} activation by removing inactivation. Equations (A3) to (A8) describe the voltage dependence and eqn (A10) the time course of activation of either a non-inactivating channel or a channel with inactivation removed. Alternatively, if an ionic channel has the property of inactivating, as with the L-type Ca^{2+} channel, the pathway to the inactivation state, S(I), must be added to the model. In such a case, the time course of

activation, $I_{Ca,O}(V,t)$ of eqn (A9), can be evaluated by setting the rate constants of the inactivation pathway to zero. Similarly, the time course of the inactivation gate closing with activation removed, $I(V,t)$, can be obtained by setting the rate constants of the activation pathway to zero. For example, in Scheme 1 in Francini *et al.* (1992), the rate constants k_5–k_{12} or k_1–k_4 must be set to zero.

Thus, the activation gate opening is obtained by subtracting the inactivation gate closing from the original current records, $I_{Ca}(V,t)$, that are the results of activation and inactivation processes (for comparison see procedure of Fig. 2 in Bezanilla & Armstrong, 1977),

$$I_{Ca,O}(V,t) = I_{Ca}(V,t) - I(V,t). \quad \text{(A20)}$$

$I_{Ca,O}(V,t)$ and $I(V,t)$ are expressed using the formalism of eqns (A3) to (A10). $I(V,t)$ is the product of the probability of closing of inactivation gates, $P_I(V,t)$, and the amplitude factor A' (eqn (A12*a*)):

$$I(V,t) = A'P_I(V,t) = A'P_I(V)P_I(t) \quad \text{(A21}a\text{)}$$

$$= A'P_I(V)\{1 - \sum_{b=1}^{b} \bar{B}_b \exp[-(t - t_0)/\tau_b]\}, \quad \text{(A21}b\text{)}$$

where $P_I(V)$ is the steady-state voltage dependence and $P_I(t)$ the time dependence of the probability of closing of inactivation gates, b corresponds to the number of time-dependent terms of the macroscopic current with time constant τ_b and $\bar{B}_b$ being the related amplitude factors. As in eqn (A10), eqn (A21*b*) must be zero at time equal to zero, so, as eqn (A13),

$$\sum_{b=1}^{b} \bar{B}_b = 1.$$

The related time course of the fraction of open channels is:

$$h(V,t) = 1 - P_I(V,t), \quad \text{(A22}a\text{)}$$

and from eqn (A21*b*):

$$h(V,t) = h(V) - (h(V) - 1)\sum_{b=1}^{b} \bar{B}_b \exp[-(t - t_0)/\tau_b]. \quad \text{(A22}b\text{)}$$

In the Hodgkin–Huxley model both activation and inactivation gates are assumed to be completely independent, therefore, if inactivation is included in the calculation, we have:

$$I_{Ca}(V) = A'm^n h^b(V), \quad \text{(A23)}$$

$$I_{Ca}(V,t) = A'm^n P_O(t) h^b(V,t), \quad \text{(A24)}$$

where $P_O(t)$ is given by eqn (A16), and

$$h^b(V,t) = \{h(V) - (h(V) - 1)\exp[-(t - t_0)/\tau_h]\}^b, \quad \text{(A25)}$$

where $h(V)$ is the steady-state inactivation variable at the test potential, b is the number of transitions in the inactivation pathway and τ_h is the time constant for inactivation. In the original Hodgkin–Huxley model $b = 1$. In eqns (A22*b*) and (A25) it is assumed that at the holding potential (−100 mV) the value of $h(-100)$ is 1.

The time course of closing of the inactivation gates, $I(V,t)$, may be obtained by either setting the rate constants of the activation pathway to zero or, from eqn (A24), fixing $mP_O(t)$ at 1. It is given by:

$$I(V,t) = A'P_I(V)\{1 - \exp[-(t - t_0)/\tau_h]\}^b. \quad \text{(A26)}$$

Evaluation of early time course of I_{Ca} activation by removing I_{ICM}. The early time course of I_{Ca} records from the edge of the 'on' voltage pulse is contaminated by I_{ICM}. Consequently, the early time course of I_{Ca} activation can be determined only by removing I_{ICM}. To this aim we adopted the following original procedure that allowed us to resolve the early time course of I_{Ca} without any evaluation or correction for I_{ICM}.

First of all we considered that I_{ICM} must have an opposite sign at 'on' and 'off', and assumed equality for 'on' and 'off' charge moving for short pulse durations. This assumption is correct if the pulse duration is very short with respect to the time constant for immobilization of intramembrane charge movement. Indeed, this is a slow phenomenon with a time constant of about 40 s (Chandler *et al.* 1976; Brum & Ríos, 1987). If it is so, for voltage pulses negative to the I_{Ca} threshold the sum of the time integral of the 'on' ($Q_{ICM,on}$) and of the 'off' ($Q_{ICM,off}$) currents must approach zero. This is confirmed by the data related to −60 mV in Fig. 4*A*. For depolarizing pulses positive to the I_{Ca} threshold we have to consider I_{Ca} activation and deactivation, $I_{Ca,on}$ and $I_{Ca,off}$, that have the same sign. Consequently, the sum of 'on' and 'off' total time integrals, $Q_{tot,on}$ and $Q_{tot,off}$, removed Q_{ICM} considering $Q_{ICM,on}$ and $Q_{ICM,off}$ equality:

$$Q_{tot,on} + Q_{tot,off} = Q_{ICM,on} + Q_{Ca,on} + Q_{ICM,off} + Q_{Ca,off}$$
$$= Q_{Ca,on} + Q_{Ca,off}, \quad \text{(A27)}$$

where $Q_{Ca,on}$ and $Q_{Ca,off}$ are the time integrals of $I_{Ca,on}$ and $I_{Ca,off}$, respectively. $Q_{Ca,on}$ includes I_{Ca} activation and inactivation, whereas $Q_{Ca,off}$ includes deactivation and recovery from inactivation. To simplify the mathematical approach and the evaluation of the results we have to take into account that I_{Ca} inactivation and recovery from inactivation are slow phenomena (Francini *et al.* 1992). Thus, for very short pulses, the time course of 'on' and 'off' currents could be considered only due to activation and deactivation of I_{Ca}. Thus, $Q_{Ca,on}$ is given by the definite 'on' time integral from time zero ('on' edge) to the end of the pulse (time duration, t). From eqn (A9) we have:

$$Q_{Ca,on} = \int_0^t I_{Ca,on}(t)\mathrm{d}t = A'P_O(V)\int_0^t P_O(t)\mathrm{d}t. \quad \text{(A28)}$$

The joined time course of $I_{Ca,off}$ has its size imposed by both the time-dependent opening probability during the pulse, $P_O(t)$, and the driving force at post-pulse potential (−100 mV in our experiments), whereas its time course is only determined by the post-pulse potential. Thus,

$$I_{Ca,off} = D'P_O(V)P_O(t)\sum_{d=1}^{d} \bar{D}_d \exp(-t_{off}/\tau_d), \quad \text{(A29)}$$

where D' is given by the Goldman–Hodgkin–Katz constant-field equation calculated at post-pulse potential, $\bar{D}_d$ are the sizes of d exponential components of I_{Ca} deactivation, with corresponding time constants τ_d that can be determined by eqn (A34*b*) as explained below. The related $Q_{Ca,off}$ is the time integral of $I_{Ca,off}$ from time zero ('off' edge) to $t_{off} \rightarrow \infty$,

$$Q_{Ca,off} = D'P_O(V)P_O(t)\int_0^{\infty} \sum_{d=1}^{d} \bar{D}_d \exp(-t_{off}/\tau_d)\,dt_{off} \quad (A30)$$

$$= D'P_O(V)P_O(t)\sum_{d=1}^{d} \bar{D}_d\tau_d.$$

Then, from eqns (A28) and (A30), eqn (A27) can be written as:

$$Q_{Ca,on} + Q_{Ca,off} = A'P_O(V)\left(DP_O(t) + \int_0^t P_O(t)dt\right), \quad (A31)$$

where,

$$D = (D'/A')\sum_{d=1}^{d} \bar{D}_d\tau_d.$$

Thus, eqn (A31) shows that eqn (A27) is simply as a function of the time course of I_{Ca} activation with its definite time integral added. Data, obtained from eqn (A31), calculated for pulses of different duration *vs.* pulse duration show a plot expressing the early time course of I_{Ca} activation with its 'running' time integral added. Thus, I_{ICM} contamination is removed without any evaluation of its time course.

Evaluation of time constants for I_{Ca} deactivation by removing I_{ICM}. In many works the deactivating (tail) current was recorded by repolarizing the membrane to test potentials after a suitable short depolarizing pulse to a voltage activating most of the ionic current under study. In some experimental conditions this procedure could be made for the scarcely contaminating I_{ICM} ($I_{ICM,off}$) but it is not suitable and correct if $I_{ICM,off}$ has size and/or duration comparable to that of the $I_{Ca,off}$. In such a case, as I_{Ca} in skeletal muscle, the time course of the tail current ($I_{tot,off}$) must be considered as a sum of two significant terms:

$$I_{tot,off}(t_{off}) = I_{ICM,off}(t_{off}) + I_{Ca,off}(t_{off}). \quad (A32)$$

Thus, $I_{ICM,off}(t_{off})$ must be removed from $I_{tot,off}(t_{off})$ to determine $I_{Ca,off}(t_{off})$. This problem can be resolved by considering that pulses with durations longer than the $I_{ICM,on}$ relaxation time move the same total charge. Consequently, using two distinct but very similar pulse durations, such as 50 and 70 ms, differences in amount of charge immobilization and I_{Ca} inactivation are very negligible, since these are slow phenomena with respect to the short interval ($\Delta t = 20$ ms) considered. Thus, for these pulse durations nearly the same total charge is moved at the 'off' and the time course of $I_{ICM,off}$ is almost equal. With this assumption, we can subtract the tail current following a 50 ms pulse from that following a 70 ms pulse to the same voltage to obtain an evaluation of $I_{Ca,off}(t_{off})$. So we have:

$$\Delta I_{Ca,off} = (I_{ICM,off,70} + I_{Ca,off,70}) - (I_{ICM,off,50} + I_{Ca,off,50})$$
$$\approx I_{Ca,off,70} - I_{Ca,off,50}. \quad (A33)$$

From eqn (A29), we have:

$$\Delta I_{Ca,off} = D'P_O(V)(P_O(t = 70) - (P_O(t = 50))$$
$$\times \sum_{d=1}^{d} \bar{D}_d \exp(-t_{off}/\tau_d), \quad (A34a)$$

that can be written in a simple form as:

$$\Delta I_{Ca,off} = aI_{Ca,off}, \quad (A34b)$$

where $a = \Delta P_O/P_O(t)$. Equations (A34*a*) and (A34*b*) show that the related time constant values are actual because they are not affected by the subtraction and that the values of factors $\bar{D}_d$ are reduced by the factor a.

Almers, W. & Palade, P. T. (1981). Slow calcium and potassium currents across frog muscle membrane: measurements with a Vaseline-gap technique. *Journal of Physiology* **312**, 159–176.

Bezanilla, F. & Armstrong, C. M. (1977). Inactivation of the sodium channel. *Journal of General Physiology* **70**, 549–566.

Brum, G., Fitts, R., Pizarro, G. & Ríos, E. (1988). Voltage sensors of the frog skeletal muscle membrane require calcium to function in excitation–contraction coupling. *Journal of Physiology* **398**, 475–505.

Brum, G. & Ríos, E. (1987). Intramembrane charge movement in frog skeletal muscle fibres. Properties of charge 2. *Journal of Physiology* **387**, 489–517.

Chandler, W. K., Rakowski, R. F. & Schneider, M. F. (1976). Effects of glycerol treatment and maintained depolarization on charge movement in frog skeletal muscle. *Journal of Physiology* **254**, 285–316.

Colquhoun, D. & Hawkes, A. G. (1977). Relaxation and fluctuations of membrane currents that flow through drug-operated channels. *Proceedings of the Royal Society* B **199**, 231–262.

Coronado, R. & Affolter, H. (1986). Characterization of dihydropyridine sensitive calcium channels from purified skeletal muscle transverse tubules. In *Ion Channel Reconstitution*, ed. Miller, C., pp. 483–505. Plenum Publishing Corp., New York.

Dirksen, R. T. & Beam, K. G. (1995). Single calcium channel behavior in native skeletal muscle. *Journal of General Physiology* **105**, 227–247.

Fabiato, A. (1988). Computer programs for calculating total from free or free from specified total ionic concentration in aqueous solution containing multiple metals and ligands. *Methods in Enzymology* **157**, 378–417.

Feldmeyer, D., Melzer, W., Pohl, B. & Zöllner, P. (1990). Fast gating kinetics of the slow Ca^{2+} current in cut skeletal muscle fibres of the frog. *Journal of Physiology* **425**, 347–367.

Feldmeyer, D., Melzer, W., Pohl, B. & Zöllner, P. (1992). Modulation of calcium current gating in frog skeletal muscle by conditioning depolarization. *Journal of Physiology* **457**, 639–653.

Feldmeyer, D., Zöllner, P., Pohl, B. & Melzer, W. (1995). Calcium current reactivation after flash photolysis of nifedipine in skeletal muscle fibres of the frog. *Journal of Physiology* **487**, 51–56.

Flockerzi, V., Oeken, H.-J., Hofmann, F., Pelzer, D., Cavalie, D. & Trautwein, W. (1986). Purified dihydropyridine-binding site from skeletal muscle t-tubules is a functional calcium channel. *Nature* **323**, 66–68.

Francini, F., Bencini, C. & Squecco, R. (1995). Slow calcium current activation in twitch skeletal muscle fibers of the frog. *Biophysical Journal* **68**, A178.

Francini, F., Pizza, L. & Traina, G. (1992). Inactivation of the slow calcium current in twitch skeletal muscle of the frog. *Journal of Physiology* **448**, 633–653.

Francini, F. & Stefani, E. (1989). Decay of the slow calcium current in twitch muscle fibers of the frog is influenced by intracellular EGTA. *Journal of General Physiology* **94**, 953–969.

García, J., Avila-Sakar, A. J. & Stefani, E. (1990). Repetitive stimulation increases the activation rate of skeletal muscle Ca^{2+} currents. *Pflügers Archiv* **416**, 210–212.

García, J., Tanabe, T. & Beam, K. J. (1994). Relationship of calcium transients to calcium currents and charge movements in myotubes expressing skeletal and cardiac dihydropyridine receptors. *Journal of General Physiology* **103**, 125–147.

Hess, P. & Tsien, R. W. (1984). Mechanism of ion permeation through calcium channels. *Nature* **309**, 453–456.

Huang, C. L.-H. (1988). Intramembrane charge movements in skeletal muscle. *Physiological Reviews* **68**, 1197–1247.

Huang, C. L.-H. (1993). Charge inactivation in the membrane of intact frog striated muscle fibres. *Journal of Physiology* **468**, 107–124.

Huang, C. L.-H. & Peachey, L. (1992). A reconstruction of charge movement during the action potential in frog skeletal muscle. *Biophysical Journal* **61**, 1133–1146.

Hui, C. S. (1991*a*). Comparison of charge movement components in intact and cut twitch fibers of the frog. *Journal of General Physiology* **98**, 287–314.

Hui, C. S. (1991*b*). Factors affecting the appearance of the hump charge movement component in frog cut twitch fibers. *Journal of General Physiology* **98**, 315–347.

Lamb, G. D. & Walsh, T. (1987). Calcium currents, charge movement and dihydropyridine binding in fast- and slow-twitch muscles of rat and rabbit. *Journal of Physiology* **393**, 595–617.

McDonald, T. F., Pelzer, S., Trautwein, W. & Pelzer, D. J. (1994). Regulation and modulation of calcium channels in cardiac, skeletal, and smooth muscle cells. *Physiological Reviews* **74**, 365–507.

Marks, T. N. & Jones, S. W. (1992). Calcium currents in the A7r5 smooth muscle-derived cell line. *Journal of General Physiology* **99**, 367–390.

Martell, A. E. & Smith, R. M. (1977). *Critical Stability Constants*, vol. III, pp. 124–126. Plenum Publishing Corporation, New York and London.

Meissner, M. (1994). Ryanodine receptor/Ca^{2+} release channels and their regulation by endogenous effectors. *Annual Review of Physiology* **56**, 485–508.

Mejía-Alvarez, R., Fill, M. & Stefani, E. (1991). Voltage-dependent inactivation of T-tubular skeletal calcium channels in planar lipid bilayers. *Journal of General Physiology* **97**, 393–412.

Meves, H. & Vogel, W. (1973). Calcium inward current in internally perfused giant axons. *Journal of Physiology* **235**, 225–265.

Ríos, E., Karhanek, M., Ma, J. & González, A. (1993). An allosteric model of the molecular interactions of excitation–contraction coupling in skeletal muscle. *Journal of General Physiology* **102**, 449–481.

Ríos, E. & Pizarro, G. (1991). Voltage sensor of excitation–contraction coupling in skeletal muscle. *Physiological Reviews* **71**, 849–908.

Sánchez, J. A. & Stefani, E. (1983). Kinetic properties of calcium channels of twitch muscle fibres of the frog. *Journal of Physiology* **337**, 1–17.

Schneider, M. F. (1994). Control of calcium release in functioning skeletal muscle fibers. *Annual Review of Physiology* **56**, 463–484.

Schwartz, L. M., McCleskey, E. W. & Almers, W. (1985). dihydropyridine receptors in muscle are voltage-dependent but most are not functional calcium channels. *Nature* **314**, 747–750.

Shirokova, N., González, A., Ma, J., Shirokov, R. & Ríos, E. (1995). Properties and roles of an intramembranous charge mobilized at high voltages in frog skeletal muscle. *Journal of Physiology* **486**, 385–400.

Simon, B. J. & Beam, K. J. (1985). The influence of transverse tubular delays on the kinetics of charge movement in mammalian skeletal muscle. *Journal of General Physiology* **85**, 21–42.

Taylor, W. R. (1988). Two-suction-electrode voltage-clamp analysis of the sustained calcium current in cat sensory neurones. *Journal of Physiology* **407**, 405–432.

Acknowledgements

The authors are most grateful to Drs A. Centonze, S. Pagannone and G. Traina for their valuable assistance in early experiments. We also wish to thank Drs M. Linari and G. Piazzesi for helpful discussion on the manuscript. This work was supported by grant no. 625 from Telethon-Italy.

Author's email address

F. Francini: francini@fisio.unifi.it

Received 14 November 1995; accepted 19 February 1996.